2016

Finding the spark: Predicting hypergolicity in ionic liquids

Caleb Michael Carlin
Iowa State University

Finding the spark: Predicting hypergolicity in ionic liquids

by

Caleb Michael Carlin

A dissertation to be submitted to the graduate faculty

in partial fulfillment of the requirements for the degree of

DOCTOR OF PHILOSOPHY

Major: Physical Chemistry

Program of Study Committee:

Mark S. Gordon, Major Professor

Theresa L. Windus

Monica H. Lamm

Thomas A. Holme

Arthur Winter

Iowa State University

Ames, Iowa

2016

TABLE OF CONTENTS

CHAPTER 1: INTRODUCTION

General Overview

The discovery of room temperature ionic liquids followed by the discovery of the versatility and range of uses for room temperature ionic liquids has spurred research in nearly every field of chemistry. The subfield ionic liquid chemistry devoted to energetic ionic liquids is particularly of interest for aerospace and military applications for use in developing ionic liquids that react with spontaneous ignition on contact with common strong oxidizers. However, the mystery of what causes some ionic liquids to have an incendiary reaction while others do not continues to elude researchers. Herein is one path to finding the secret of hypergolic ionic liquids.

Dissertation Overview

Chapter 1 introduces the fundamental concepts necessary to understand ab initio calculations and ionic liquid chemistry. The methods to be used in later chapters are also introduced and detailed on a fundamental level. Chapter 2 investigates the proton affinity and first ionization potential of energetic ionic liquid anions as well as testing the computational costs of MP2 and CR-CC(2,3) vs. accuracy. Chapter 3 continues the work of chapter 2 with an investigation of energetic ionic liquid cations as well as the energy released when a proton is transferred from the cation to the anion. The implications of the proton transfer reaction are considered in the context of predicting hypergolicity. Chapter 4 covers the development of a fully quantum mechanical Metropolis Monte

Carlo method and the implementation of that method in GAMESS. Chapter 5 introduces and derives a new method for calculating the equilibrium constant of a proton transfer reaction in the condensed phase. Chapter 6 concludes the thesis with a summary of the results of the previous chapters.

Theoretical Background

The study of quantum chemistry concerns itself primarily with finding approximate solutions to the Schrödinger Equation, which mathematically relates the state of nuclei and electrons to the total energy of the system. In most cases, this involves solving the time-independent Schrödinger Equation[1].

$$\hat{H}|\Phi\rangle = E|\Phi\rangle \tag{1}$$

Here $\hat{H}$ is the Hamiltonian operator for the system of nuclei and electrons, $|\Phi\rangle$ is the wavefunction, and E is the total energy of the system. The general Hamiltonian can be written as electronic, nuclear, and combined terms.

$$\hat{H} = \left(-\tfrac{1}{2}\sum_{i=1}^{n}\nabla_i^2 + \sum_{i=1}^{n}\sum_{j>i}^{n}\frac{1}{r_{ij}} \right) + \left(-\sum_{p=1}^{N}\frac{1}{2M_p}\nabla_p^2 + \sum_{p=1}^{N}\sum_{q>p}^{N}\frac{Z_p Z_q}{r_{pq}} \right) - \sum_{i=1}^{n}\sum_{p=1}^{N}\frac{Z_p}{r_{ip}} \tag{2}$$

The Laplacian operator, defined as $\nabla^2 f = \sum_{i=1}^{n}\frac{\partial^2 f}{\partial x_i^2}$, appears in the kinetic energy terms.

The sums *n* and *N* are over all electrons and nuclei respectively and r_{xy} is the separation between x and y of the form $|r_x - r_y|$. The $\frac{1}{r}$ terms correspond to the attractive and repulsive potential energy terms arising from electron and nuclei interactions. The mass and charge of the nuclei are given by M_p and Z_p respectively.

Key to the application of quantum chemistry is the Born-Oppenheimer approximation[2] that decouples the movement of nuclei and electrons due to the difference in mass and speed. With this approximation, the nuclei are treated to be stationary with regard to the motion of electrons and equation 2 reduces to

$$\hat{H}_{electron} = -\tfrac{1}{2}\sum_{i=1}^{n}\nabla_i^2 + \sum_{i=1}^{n}\sum_{j>i}^{n}\frac{1}{r_{ij}} - \sum_{i=1}^{n}\sum_{p=1}^{N}\frac{Z_p}{r_{ip}} \tag{3}$$

as the terms that only involve the nuclei either go to zero (nuclear kinetic energy) or become constants (nuclear-nuclear repulsion) that don't affect the wavefunction solutions to the Schrödinger equation. While the Born-Oppenheimer approximation significantly simplifies the Schrödinger equation, the many body problem still remains for systems with two or more electrons, and further approximation is necessary.

One approximate solution of the Schrödinger equation is an antisymmetrized Hartree product of spin orbitals that minimizes the total energy in accordance with the variational principle. Spin orbitals, the product of a spatial orbital and spin function, each describe the behavior of a single electron such that the full wavefuction is written as a Slater determinant[3] to ensure that the wavefunction is antisymmetric when any two electrons are interchanged. Within the Hartree-Fock approximation[4], the Hamiltonian is replaced with a one-electron operator and a potential energy term that averages out the interaction between the electron and all other electrons.

$$\hat{F}_i^{HF}\chi_i = \hat{h}_i\chi_i + \sum_j \hat{J}_j\chi_i - \sum_j \hat{K}_j\chi_i = \varepsilon_i\chi_i$$
$$\hat{h}_i = -\tfrac{1}{2}\nabla_i^2 - \sum_p \frac{Z_p}{r_{ip}} \tag{4}$$

The indices i and j correspond with the spin orbitals (χ) representing the electrons. The Coulomb operator $\hat{J}$ yields the average repulsive interaction between a given electron in the field of the other electrons, and the exchange operator $\hat{K}$ accounts for the purely quantum change in energy that arises due to interchanging electrons between two different spin orbitals. Combining these operators yields the Fock operator and the compact form of the Hartree-Fock equation.

$$\hat{F}_i \chi_i = \varepsilon_i \chi_i \tag{5}$$

To define the spatial orbitals used in creating the spin orbitals, a basis set of spatial functions is introduced, generally chosen so that the basis set is not orthonormal. The spatial orbital (ψ) is a linear combination of the basis functions (ϕ) determined by the coefficients C.

$$\psi_i = \sum_u C_{ui} \phi_u \tag{6}$$

The Fock operator does not operate on the spin function, so substituting equation (6) in to equation (5), multiplying on the left on both sides on the equation, and integrating over all space leads to the Roothan-Hall matrix equation[5].

$$\begin{aligned} FC &= SC\varepsilon \\ F_{uv} &= \int \phi_{vi}^* \hat{F}_i \phi_{ui} dr \\ S_{uv} &= \int \phi_{vi}^* \phi_{ui} dr \end{aligned} \tag{7}$$

As before, the index i corresponds to the spin orbital operated on by the Fock operator. The Fock operator and coefficients are replaced with the matrices F and C respectively

and the overlap matrix S is introduced. The energies of each orbital are given by the non-zero elements in the diagonal matrix ε. The Roothan-Hall equation can be solved by using standard matrix techniques but because the Fock matrix depends on the coefficients, the solution must be solved iteratively. An initial guess for the coefficients is used to solve for a new set of coefficients and the process is repeated until the change in the coefficients falls below a specified threshold. The process is called the self-consistent field method.

The averaged way that Hartree-Fock treats the electron-electron interactions fails to capture the instantaneous interactions called electron correlation, defined as the difference between the exact non-relativistic energy and the Hartree-Fock energy. One method for calculating the correlation energy is to rewrite the Hamiltonian as the Hartree-Fock Hamiltonian plus a perturbation of the potential that can be made arbitrarily small by varying a parameter.

$$\hat{H} = \hat{H}_{HF} + \lambda V_{Pert} \tag{8}$$

The wavefunction and energy are eigenfunctions and eigenvalues respectively of the Hamiltonian and so are dependent on the parameter λ and can be expanded in a Taylor series in powers of λ.

$$\begin{aligned} \Psi(\lambda, r) &= \Psi\big|_{\lambda=0} + \left.\frac{\partial \Psi}{\partial \lambda}\right|_{\lambda=0} \lambda + \left.\frac{\partial^2 \Psi}{\partial \lambda^2}\right|_{\lambda=0} \lambda^2 + \ldots \\ E(\lambda) &= E\big|_{\lambda=0} + \left.\frac{d\, E}{d\lambda}\right|_{\lambda=0} \lambda + \left.\frac{d^2 E}{d\lambda^2}\right|_{\lambda=0} \lambda^2 + \ldots \end{aligned} \tag{9}$$

Substituting the two expansions into the Schrödinger equation, terms with equal powers of λ on both sides of the equation must be equal for all values of λ. The zeroth power of λ is the Hartree-Fock equation for the unperturbed system. The first power of λ term does not contribute to the correlation energy as it involves interactions between the ground state and singly excited determinants, which by the Brillouin theorem is zero[6]. Thus the second power of λ is the first to contribute to the electron correlation and the second order correction to the total energy $E^{(2)}$ is given by equation 10.

$$E^{(2)} = \sum_{d} \frac{\left| \left\langle \Psi_d \left| V_{pert} \right| \Psi_{GS} \right\rangle \right|^2}{E_d^{(0)} - E_{GS}^{(0)}} \tag{10}$$

The summation is over all double excitations d, Ψ_d and Ψ_{GS} are the doubly excited and ground state determinants, and $E_d^{(0)}$ and $E_{GS}^{(0)}$ are the corresponding zeroth order energies of Ψ_d and Ψ_{GS}. Adding $E^{(2)}$ to the Hartee-Fock energy yields the Möller-Plesset second order perturbation (MP2) energy[7].

The coupled cluster method[8,9] is a post-Hartree-Fock method that approximates the exact wave function as a reference wavefunction acted on by exponential excitation operators. While the reference wavefunction is often a Slater determinant resulting from a Hartree-Fock calculation, it is not necessary that this be the case.

$$\Psi_{exact} = e^{\hat{T}} \psi_{ref} \tag{11}$$

The excitation operator $\hat{T}$ is a series of particle operators that operate on one or more electron to excite from occupied orbitals to unoccupied virtual orbitals.

$$\hat{T} = \hat{T}_1 + \hat{T}_2 + \hat{T}_3 + \ldots$$
$$\hat{T}_1 = \sum_{i,a} t_i^a \hat{t}_i^a \qquad (12)$$
$$\hat{T}_2 = \sum_{i<j} \sum_{a<b} t_{ij}^{ab} \hat{t}_i^a \hat{t}_j^b$$

The sums run over all single and non-duplicate double excitations from occupied orbitals (i, j) to virtual orbitals (a, b) for the single electron operators $\hat{t}$. In the case where the series is truncated after double excitations, the coefficents t_i^a and t_{ij}^{ab} are calculated via matrix operations to give the couple cluster singles and doubles (CCSD) correction to the energy. The energies obtained using the coupled cluster methods are more accurate than MP2 and can be further improved by truncating the operator series after larger numbers of excitations, however the increase in accuracy comes with increased computational costs. MP2 formally scales with the size of the basis set as N^5 and CCSD scales as N^6. Coupled cluster with single, double, and triple excitations (CCSDT) scales as N^8 although calculating the triple excitation coefficients non-iteratively (CCSD(T)) reduces the scaling to N^7.[10]

The completely renormalized left-eigenstate coupled-cluster method with double and triple excitations (CR-CCSD(T)$_L$) is an improvement on previous coupled-cluster methods for systems involving large non-dynamic correlation effects like biradicals and bond breaking[11]. Starting from the CC wavefunction defined in equation 11, the ground state energy E_0 is renormalized to account for singularities in the potential energy that arise at large internuclear distances when using many body perturbation theory[12].

$$E_0 = \frac{\langle \Psi_{CC} | \hat{H} e^{\hat{T}} | \psi_{ref} \rangle}{\langle \Psi_{CC} | e^{\hat{T}} | \psi_{ref} \rangle} \qquad (13)$$

Introducing a de-excitation operator analogous to $\hat{T}$ that operates on the left (the bra) for excitations beyond the truncation of $\hat{T}$, the left eigenstates and eigenfunctions are determined via equation 14.

$$\langle \Psi_{CC} | \hat{L}_0 \bar{H} = E_0 \langle \Psi_{CC} | \hat{L}_0$$
$$\bar{H} = e^{-\hat{T}} \hat{H} e^{\hat{T}} \qquad (14)$$

The deexcitation operator $\hat{L}_0$ is then used to determine the correction to the CC energy by non-iterative means. For CR- CCSD(T)$_L$, the truncation for the CC energy is after the double excitations term and the triple excitations term is solved non-iteratively using the left eigenstate operator. CR-CCSD(T)$_L$ scales as N^7 as does CCSD(T).

One strategy to reduce the computational cost of a calculation when the scaling of the method has been reduced as far as possible is to fragment the system into subsystems, each representing a much smaller N size, and then calculating some subset of the total interactions between the subsystems. One such method is the fragment molecular orbital method (FMO) that allows for intra-molecular and intermolecular fragmentation[13,14]. The electron density of the fragments or monomers are calculated separately within the potential field of the rest of the system, iterating over the monomers to self-consistency. The inter-monomer interactions can then be calculated for dimers (FMO2), trimers (FMO3), or higher number of interacting fragments using the monomer electron densities and the potential field of the system, treating each multi-fragment interaction as a

perturbation to the monomer energy. The total energy is then the summation over the monomer and other calculated terms in the n-body expansion. For large systems where short range interactions dominate, the calculation cost can be further reduced by replacing multi-fragment interactions separated by more than a cutoff distance with a model potential.

Another method for reducing the computational costs is to replace some or all molecules with parameterized models such as the Effective Fragment Potential method (EFP)[15-18]. Developed initially to describe spectator molecules around solvated molecules, EFP uses parameters derived entirely from ab initio calculations with no empirical fitting of parameters. Intermolecular interactions are calculated using multipolar expansions at points distributed across the EFP molecule, generally at the center of each atom and the midpoint of each bond. Inter-fragment interactions are calculated classically while fragment-ab initio interactions are treated as a perturbation in the Hamiltonian of the ab initio region of the system with the polarization of the solvent and solute solved by iterating the induced polarization of the fragments to self-consistency. The original EFP1 implementation includes parameters for water while the

more general EFP2 allows for parameterizing any molecule for use as a EFP fragment through a series of ab initio calculations.

The Monte Carlo method is a broad range of techniques that involve random sampling of values to locate the desired solution by means of a probabilistic model[19,20]. The development of computers capable of performing the large number of repetitive calculations necessary allowed the reintroduction and development of the modern Monte Carlo method[21]. Originally developed for the study of nuclear physics during the Manhattan Project, the Monte Carlo method is an important tool for studying potential energy surfaces and generating ensembles for chemical systems as it only requires calculating the total energy of the system. The Metropolis Monte Carlo method is one of many variations of the Monte Carlo method that is characterized by the use of Markov Chains and the Boltzmann factor as defined by equation 15.

$$P = e^{\frac{-\Delta E}{kT}} \tag{15}$$

Here P determines the probability that a new step in the Markov Chain will be accepted or rejected based on the change in energy $\Delta E = E_{new} - E_{old}$ divided by the Boltzmann constant k and the temperature T. If the energy of the new step is less than the previous step, then the new step is accepted. If the energy of the new step is greater than the previous step, then the new step is accepted if a random number is greater than P otherwise the step is rejected. Effective for finding minima on the potential energy

surface and generating ensembles that follow the Boltzmann distribution, the Monte Carlo method is limited to non-dynamic properties.

A Metropolis Monte Carlo simulation is dependent only on the temperature and the starting configuration of the atoms. In situations where a particular portion of the configurational phase space is of interest it is beneficial to introduce additional constraints on the Monte Carlo simulation. As the constraint biases the probability of some states over others, use of the Boltzmann factor is no longer sufficient to ensure that a valid ensemble will be generated[22]. Instead each constraint adds a weighting function that changes the distribution of states and must be accounted for in the acceptance factor or by un-weighting the results after the Monte Carlo simulation is finished. One constraint method, termed umbrella sampling, involves the addition of a potential that biases the Markov chain to increase sampling in areas that would otherwise be under sampled by unconstrained Monte Carlo[23]. Results are obtained by integrating the states of one or more regions sampled using umbrella potentials by applying an un-weighting function. Another method of biasing the Monte Carlo simulation is to change the internal configuration of molecules to increase sampling of low energy states[24,25]. For example, the Configurational-Bias Monte Carlo (CBMC) designed for long chain molecules generates the next step in the Markov Chain by inserting the molecule in a piecewise fashion, trying multiple configurations for each piece and accepting the lowest energy configuration[26]. The acceptance criteria for CBMC is formulated to incorporate the energy of each of the rejected trial configurations of each piece of the inserted molecule. A third constraint method is to reduce the degrees of freedom of the chemical system by prohibiting some of the possible perturbations when generating a new step in the Markov

Chain[27]. Whether by prohibiting the motion of entire molecules or a single bond, such a constraint limits the sampling of the potential energy surface to some subset of the full surface, allowing for an unbiased sampling in that subset. As the extent of the bias is unique to the choice of which perturbations are prohibited, the acceptance criteria must be determined for each system separately unlike the more general forms used for umbrella sampling and CBMC.

In the 1920's, development of liquid fuel rocket engines was undertaken around the world resulting in discovery of hypergolic fuels in the Soviet Union, Germany, and the United States between 1930 and 1940[28]. A hypergolic fuel or bipropellant is a pair of liquids that spontaneously ignite upon contact. The early experiments focused on organic compounds reacting with nitric acid for use as the main rocket fuel or as the initial stage to provide the temperature and pressure necessary for igniting other fuels. At present the most commonly used hypergolic combination is dinitrogen tetroxide with hydrazine or related oxidizer, which is considered extremely toxic and corrosive[29]. Efforts to identify suitable replacement hypergolic fuels that provide the same utility without the chemical hazards have turned to a class of chemicals called ionic liquids.

A class of compounds synthesized from ions with melting points below 100 °C are called ionic liquids or room temperature ionic liquids to differentiate from high

temperature molten inorganic salts[30]. Typically, ionic liquids are composed of bulky, asymmetric cations paired with weakly coordinating anions resulting in weak lattice energies. Depending on the specific cation and anion combination, ionic liquids have been shown to have wide ranging physical and chemical properties that allow for fine tuning the choice of ionic liquid for practical applications[31-34]. The underlying chemistry that governs the observed variations in ionic liquids are not yet fully understood well enough to predict the properties of a given ionic liquid. It has been shown that non-Coulombic, non-covalent interactions like dispersion make up a significant portion of the intermolecular interactions of ionic liquids, necessitating the use of accurate quantum methods when studying ionic liquids computationally[35].

It has been demonstrated that some energy dense ionic liquids react hypergolically with white fuming nitric acid and/or hydrogen peroxide[29]. The hypergolic ionic liquids determined at present are nitrogen rich, protic ionic liquids, meaning the charge carrier between cation and anion is a proton[32]. Experimental studies have demonstrated the importance of the proton transfer from the cation to the anion as a first step in the hypergolic decomposition reaction[36]. Further studies have shown that protic ionic liquids generally exist as a neutral pair in the vapor phase while aprotic ionic

liquids generally exist as ion pairs in the vapor phase[37,38]. The interaction between liquid and vapor phase is important as high speed measurements of ionic liquids dropped into white fuming nitric acid show the evolution of a vapor phase followed by ignition in the phase[39].

References

1) (a) Schrödinger, E. Ann. Phys. 1926, 79, 361. (b) Schrödinger, E. Ann. Phys., 1926, 79, 489. (c) Schrödinger, E. Ann. Phys., 1926, 79, 734. (d) Schrödinger, E. Ann. Phys., 1926, 80, 437. (e) Schrödinger, E. Ann. Phys., 1926, 81, 109. (f) Schrödinger, E. Die Naturwissenschaften, 1926, 14, 664.

2) Born, M; Oppenheimer, R. Ann. Phys., 1927, 84, 457.

3) Slater, J. C. Phys. Rev., 1929, 34, 1293.

4) (a) Hartree, D. R. Proc. Cambridge Philos. Soc., 1928, 24, 89. (b) Hartree, D. R. Proc. Cambridge Philos. Soc., 1928, 24, 111. (c) Hartree, D. R. Proc. Cambridge Philos. Soc., 1928, 24, 426. (d) Fock, V. Z. Phys.,
1930, 61, 126. (e) Fock, V. Z. Phys., 1930, 62, 795.

5) Roothaan, C. C. J. Reviews of modern physics 23, no. 2 (1951): 69.

6) Brillouin, L. J. Phys., Paris, 3, 373 (1932)

7) Møller, C.; Plesset, M. S. Phys. Rev. 1934, 46, 618.

8) Cizek,J. J. Chem. Phys. 45, 4256 (1966).

9) Cizek, J. Adv. Chem. Phys. 14, 35 (1969).

10) Shavitt, I.; Bartlett, R. J. *Many-Body Methods in Chemistry and Physics: MBPT and Coupled-Cluster Theory.* Cambridge University Press 2009

11) Piecuch, P.; Wloch, M. J. Chem. Phys. 123, 224105 (2005)

12) Piecuch, P.; Kowalski, K.; Pimienta, I. S. O.; Mcguire, M. J. Int. Rev. Phys. Chem. 21, 527-655 (2002)

13) Kitaura, K.; Ikeo, E.; Asada, T.; Nakano, T.; Uebayasi, M. Chem. Phys. Lett. 313, 701-706 (1999)

14) Gordon, M. S.; Fedorov, D. G.; Pruitt, S. R.; Slipchenko, L. V. Chem. Rev. 112, 632-672 (2012)

15) Jensen, J. H.; Day, P. N.; Gordon, M. S.; Basch, H.; Cohen, D.; Garmer, D. R.; Kraus, M.; Stevens, W. J. Modeling the Hydrogen Bond, 569, 139–151 (1994)

16) Day, P. N.; Jensen, J. H.; Gordon, M. S.; Webb, S. P.; Stevens, W. J.; Krauss, M.; Garmer, D.; Basch, H.; Cohen, D. J. Chem. Phys. 105, 1968-1986 (1996)

17) Gordon, M. S.; Freitag, M. A.; Bandyopadhyay, P.; Jensen, J. H.; Kairys, V.; Stevens, W. J. J. Phys. Chem. A 105, 293-307 (2001)

18) Gordon, M. S.; Slipchenko, L. V.; Li, H.; Jensen, J.H.. Annual Reports in Computational Chemistry, 3, 177-193 (2007).

19) Metropolis, N. and Ulam, S. J. Am. Stat. Assoc. 44, 335-341 (1949)

20) Metropolis, N.; Rosenbluth, A. W.; Rosenbluth, M. N.; Teller, A. H. J. Chem. Phys. 21, 1087-1092 (1953)

21) Metropolis, N. Los Alamos Science Special Issue. 125-130 (1987)

22) Theodorou, D. N. J. Chem. Phys. 124, 034109 (2006)

23) Torrie, G. M. and Valleau, J. P. J. Comp. Phys. 23, 187-199 (1977)

24) Rosenbluth, M. N. and Rosenbluth, A. W. J. Chem. Phys. 23, 356 (1955)

25) Martin, M. G. and Ilja Siepmann, J. J Phys. Chem. B. 103, 4508-4517 (1999)

26) Maginn, E. J.; Bell, A. T.; Theodorou, D. N. J. Phys. Chem. 99, 2057-2079 (1995)

27) Asselin, P.; Evans, R. F. L.; Barker, J.; Chantrell, R. W.; Yanes, R.; Chubykalo-Fesenko, O.; Hinzke, D.; Nowak, U. Phys. Rev. B. 82, 054415 (2010)

28) Sutton, G. P. J. Prop. Pow. 19, 978-1007 (2003)

29) Schneider, S.; Hawkins, T.; Ahmed, Y.; Rosander, M.; Mills, J.; Hudgens L. Agnew. Chem. Int. Ed. 123, 6008-6010 (2011)

30) C. F. Poole, J. Chromatogr. A 2004, 1037, 49–82

31) K. Dong, S. Zhang, Chem. Eur. J. 2012, 18, 2748-2761

32) T. L. Greaves, C. J. Drummond, Chem. Rev. 2008, 108, 206-237

33) J. A. Bautista-Martinez, L.Tang, J. -P. Belieres, R. Zeller, C. A. Angell, C. Friesen, J. Phys. Chem. C, 2009, 113, 12586-12593

34) C. A. Angell, N. Byrne, J. -P. Belieres, Acc. Chem. Res. 2007, 40, 1228-1236

35) Izgorodina, E. I.; Goize, D.; Maganti, R.; Armel, V.; Taige, M.; Schubert, T. J. S.; MacFarlane, D. R. Phys. Chem. Chem. Phys. 16, 7209-7221 (2014)

36) Chambreau, S. D.; Schneider, S.; Rosander, M.; Hawkins, T.; Gallegos, C. J.; Pastewait, M. F.; Vaghjiani, G. L. J. Phys. Chem. A. 112, 7816-7824 (2008)

37) Deyko, A.; Lovelock, K. R. J.; Licence, P.; Jones, R. G. Phys. Chem. Chem. Phys. 13, 16841-16850 (2011)

38) Leal, J. P.; Esperanca, J. M. S. S.; Minas da Piedade, M. E.; Canongia Lopes, J. N.; Rebelo, L. P. N.; Seddon, K. R. J. Phys. Chem. A. 111, 6176-6182 (2007)

39) Chowdhury, A.; Bapat, C.; Thynell, S. T. Rev. Sci. Instrum. 80, 044101 (2009)

CHAPTER 2: AB INITIO CALCULATION OF ANION PROTON AFFINITY AND IONIZATION POTENTIAL FOR ENERGETIC IONIC LIQUIDS

A paper published in the *Journal of Computational Chemistry*

Caleb Carlin and Mark S. Gordon

Abstract

Developing a better understanding of the bulk properties of ionic liquids requires accurate measurements of the underlying molecular properties that help to determine the bulk behavior. Two computational methods are used in this work: second order perturbation theory (MP2) and completely renormalized coupled cluster theory (CR-CC(2,3)), to calculate the proton affinity and ionization potential of a set of anions that are of interest for use in protic, energetic ionic liquids. Compared with experimental values, both methods predict similarly accurate proton affinities, but CR-CC(2,3) predicts significantly more accurate ionization potentials. It is concluded that more time intensive methods like CR-CC(2,3) are required in calculations involving open shell states like the ionization potential.

Introduction

Room temperature molten salts, or ionic liquids (ILs), as a class exhibit a wide range of thermodynamic and physical properties[1]. The potential applications of ILs in fields such as aerospace, chemical synthesis, and fuel cells may be as numerous as the number of possible cation-anion combinations used to make ILs. It is for this reason that a great deal of interest exists not only in synthesizing new ILs, but also in gaining a better understanding of the underlying chemistry that can lead to a set of rules that can be used to predict the properties of a given IL[2]. A growing body of research has focused on the

nature of non-covalent interactions in bulk ILs, for example, by analyzing the role of hydrogen bonding in the determination of IL properties[3-6]. Non-covalent interactions have been shown to be important determinants of properties like vapor pressure, viscosity, melting temperature, density, solubility, and conductivity[6-9]. Attempts to characterize the interactions, both experimentally and computationally, have suggested that ILs exist in the liquid phase as an equilibrium between (a) charged ions that are stabilized by non-bonded interactions and (b) neutral molecules, with the location of a charge carrier as the difference[7,8,10]. For protic ionic liquids (PILs), a subset of ILs formed by combining a Brønsted acid and base, the charge carrier is a proton. PILs are a focus of theoretical research for the relative simplicity of the reversible proton transfer reaction between the ions[7]. One proposed set of determining factors for the proton transfer reaction equilibrium is the acidity of the donor and the proton affinity (PA) of the acceptor[8,11,12]. In working toward testing this hypothesis, the present work discusses methods for calculating proton affinities with an accuracy that is sufficient to provide insight about IL properties.

The PA of anions can be determined from indirect experimental measurements and by computations. Experimentally, anion PAs can be obtained using thermodynamic cycles and an experimentally determined first electron affinity, or by comparing the gas phase acidity of the anion to the gas phase acidity of anions with known PAs[13-15]. While these methods have provided a narrow range of upper and lower bounds for the PAs of a few anions of interest, the paucity of experimental data limits the number of species for which these experimental approaches are applicable. Computational methods provide a direct way to calculate the PA; the error in the calculations is dependent on the level of

theory and basis set used. Previous studies using Møller-Plesset second order perturbation (MP2)[16] theory have predicted PAs of small organic anions with errors on the order of 0.1 eV[17,18,19,20,21]. Izgorodina, Forsyth, and MacFarlane probed the relative electron delocalization of anions using PAs calculated with the coupled cluster singles, doubles, and non-iterative triples (CCSD(T)) method and with the same atomic basis set used in the present work[19]. The completely renormalized left eigenstate coupled cluster method with single and double excitations, plus non-iterative triples (CR-CC(2,3))[22] is employed in the present study. Previous studies have shown that the CR-CC(2,3) method has a computational cost that is comparable to that of CCSD(T) and is generally at least as accurate as CCSD(T). For systems in which there is significant diradical character (e.g., for single bond breaking processes), the CR-CC(2,3) method is considerably more accurate than CCSD(T)[23].

The first ionization potential (IP) of an anion provides another test for theory and potentially another method to assess properties of ionic liquids. Previous studies have reported direct measurements of the ionization potential of an anion using UV spectroscopy[13,24,25]. One of the UV spectroscopy studies demonstrated that for the studied anions there is a negligible difference between the vertical and adiabatic ionization potential and concluded that the same would likely hold true in general[13]. For this reason, only the vertical ionization potentials are presented here. For the PAs, both the geometries of the anion and the neutral species have been fully optimized.

Previous work in which calculated anion IPs are reported has focused on inexpensive semi-empirical and density functional theory (DFT) methods. For example, Kita et. al. used MNDO and Koopmans Theorem to approximate the IPs of anions in

organic lithium salts[26-27]. Ue, Murakami, and Nakamura found that using Koopmans theorem to approximate the vertical IP of anions using Hartree-Fock orbital energies overestimates the IPs by about 3 eV compared to adiabatic IPs calculated using DFT with the B3LYP functional and the 6-311+G(2d,p) basis set[28-32]. Borodin and Smith reported that a large basis set with diffuse functions is necessary to reproduce anion IPs[33]. A rigorous study by Johansson confirmed the results of Kita and Ue by calculating the IPs of a wide range of anions using semi-empirical methods, Hartree-Fock, and three DFT functionals[34,35]. The present work addresses the computation of both Pas and IPs using post-Hartree-Fock methods.

Computational Methods

All calculations were performed using the GAMESS[22,36,37] software package. Both the MP2 and CR-CC(2,3) calculations employed the augmented correlation consistent triple zeta (aug-cc-pVTZ)[38,39] basis set. Geometries were determined by MP2 geometry optimizations and confirmed as minima by calculating and diagonalizing the Hessian matrix of energy second derivatives. Energy calculations at these optimized geometries for the anionic and neutral species were done with both CR-CC(2,3) and MP2. The open shell energies were calculated using the restricted open shell Hartree-Fock method with electron correlation obtained using CR-CC(2,3) and Z-averaged second order perturbation theory (ZAPT2[40]) at the optimized geometry of the anion. The IP and PA are taken to be

$$E_{IP} = E_{neutral} - E_{anion}$$

$$E_{PA} = E_{anion} - E_{protonated}$$

so that both the IP and PA are positive. The zero point energy (ZPE) correction is not needed for the vertical IP calculations, but is included for the PA calculation using the frequencies calculated from the MP2 Hessian matrix.

Results and Discussion

The anions studied in this work, chosen based on available experimental data and on their potential use in energetic ionic liquids, are dinitramide, dicyanamide, nitrate, perchlorate, azide, phosphinate, borohydride, cyanoborohydride, and dicyanoborohydride (Figure 1). Table 1 compares the predicted and experimental PAs, both with and without the ZPE contribution, sorted in order of decreasing CR-CC(2,3) PA. PAs predicted by both MP2 and CR-CC(2,3) are in reasonable agreement with the experimental values. MP2 and CR-CC(2,3) produce similar predicted PAs, because no open shell species are involved in the PA calculations. Azide is a special case, as the anion is linear while the protonated molecule is not. This results in a change in the rotational energy that is not included here[17]. Table 2 presents the calculated and experimental IPs using the same ordering scheme as in Table 1. For the anions for which experimental data are available, the CR-CC(2,3) IPs are considerably more accurate than are those predicted by MP2. For the azide IP, the CR-CC(2,3) results are comparable to the multi-reference CASPT2 method[41]. Tables 1 and 2 include previously reported calculated PAs for the nitrate, dinitramide, and dicyanamide anions and previously reported calculated IPs for the azide and percholate anions. The MP2/cc-pVDZ nitrate PA differs from experiment by 0.97 eV more than does the present work[45], likely due to the use of a smaller basis set in the previous calculations.

The calculated CR-CC(2,3) IP for ClO_4^- has a greater error relative to experiment than do the IPs for the other anions for which experimental data are available. The MP2 ClO_4^- IP is similar to that predicted by CR-CC(2,3). The reason for the relatively poorer performance of CR-CC(2,3) for ClO_4^- may be attributed, at least in part, to the Jahn-Teller effect that occurs in T_d symmetry when the excess electron is removed. While the triply degenerate set of highest occupied molecular orbitals (HOMO) is fully occupied with six electons in the anion, the occupancy of the HOMO orbitals is only five electrons in the neutral, after the excess electron is removed. This occurrence is easily treated using state-averaged multi-configurational methods, but for single configuration-based methods, it is common to use a subgroup of T_d, such as C_{2v}, as was done with the B3LYP method in reference 42. The same subgroup approach was used for the MP2 and CR-CC(2,3) calculations in the present work. The B3LYP IP for ClO_4^- is in better agreement with experiment than are the values predicted by the *ab initio* methods used in the present work[42]. This is likely due to a fortunate cancellation of errors in the B3LYP calculations[43,44].

Conclusion

In this work, two methods were used to calculate the PAs and IPs for a set of anions to determine the accuracy and efficiency of both methods. It has been demonstrated that both MP2 and CR-CC(2,3) produce PAs with similar accuracy compared to experiment. Therefore, the less computationally demanding MP2 method appears to be reliable for the prediction of ionic liquid PAs. For IPs, the CR-CC(2,3) method produces significantly more accurate values compared to experiment than does MP2. For most species studied, the CR-CC(2,3) method predicts IPs that are in good

agreement with the experimental values. However, for molecules that have degenerate frontier orbitals, such as ClO_4^-, it is important to use a multi-configuration reference wave function, in order to accommodate fractional orbital occupancy.

Acknowledgements

This material is based upon work supported by the Air Force Office of Scientific Research under AFOSR Award No. FA9550-11-1-0099.

References

1. C. F. Poole, J. Chromatogr. A **2004**, 1037, 49–82

2. Y. Zhang, H. X. Gao, Y. -H. Joo, J. M. Shreeve, Angew. Chem. Int. Ed. **2011**, 50, 9554 – 9562

3. M. A. Gebbie, M. Valtiner, X. Banquy, E. T. Fox, W. A. Hendeson, J. N. Israelachvili, PNAS **2013**, 110, 9674-9679

4. E. I. Izgorodina, D. R. MacFarlane, J. Phys. Chem. B **2011**, 115, 14659-14667

5. S. A. Katsyuba, M. V. Vener, E. E. Zvereva, Z. Fei, R. Scopelliti, G. Laurenczy, N. Yan, E. Paunescu, P. J. Dyson, J. Phys. Chem. B. **2013**, 117, 9094-9105

6. K. Dong, S. Zhang, Chem. Eur. J. **2012**, 18, 2748-2761

7. T. L. Greaves, C. J. Drummond, Chem. Rev. **2008**, 108, 206-237

8. J. A. Bautista-Martinez, L.Tang, J. -P. Belieres, R. Zeller, C. A. Angell, C. Friesen, J. Phys. Chem. C, **2009**, 113, 12586-12593

9. C. A. Angell, N. Byrne, J. -P. Belieres, Acc. Chem. Res. **2007**, 40, 1228-1236

10. J. Stoimenovski, E. I. Izgorodina, D. R. MacFarlane, Phys. Chem. Chem. Phys. **2010**, 12, 10341-10347

11. P. C. Singh, G. N. Patwari, J. Phys. Chem. A **2007**, 111, 3178-3183

12. T. Zeegers-huyskens, J. Mol. Struct. **1988**, 177, 125-141

13. X. Yang, B. Kiran, X. -B. Wang, L. -S. Wang, M. Mucha, P. Jungwirth, J. Phys. Chem. A **2004**, 108, 7820-7826

14. M. J. Pellerite, R. L. Jackson, J. I. Brauman, J. Phys. Chem. **1981**, 85, 1624-1626

15. J. A. Davidson, F. C. Fehsenfeld, C. J. Howard, Int. J. Chem. Kinet. **1977**, 9, 17-29

16. C. Moller, M. S. Plesset, Phys. Rev. Lett. **1934**, 46, 618−621

17. J. K. Labanowski, R. A. Hill, D. J. Heisterbergy, D. D. Miller, C. F. Bender, J. W. Andzelm, Proton affinities calculated by traditional ab initio approaches and by density functional methods. http://www.ccl.net/cca/documents/proton-affinity/affinities.pdf. (Accessed August 18, 2014)

18. M. Meot-Ner, J. F. Liebman, J. E. Del Bene, J. Org. Chem. **1986**, 51, 1105-1110

19. E. I. Izgorodina, M. Forsyth, D. R. MacFarlane, Aust. J. Chem. **2007**, 60, 15–20

20. J. Chandrasekhar, J. G. Andrade, P. von Rague Schleyer, J. Am. Chem. Soc. **1981**, 103, 5609-5612

21. J. E. Del Bene, J. Phys. Chem. **1993**, 97, 107-110

22. K. Kowalski, P. Piecuch, J. Chem. Phys. **2004**, 120, 1715−1738

23. (a) S. A. Nedd, N. J. DeYonker, A. K. Wilson, M. S. Gordon, P. Piecuch, J. Chem. Phys. **2012**, 136, 144109; (b) Y. Ge, M. S. Gordon, P. Piecuch, J. Chem. Phys., **2007**, 127, 174106; (c) Y. Ge, M. S. Gordon, P. Piecuch, M. Wloch, J. R. Gour, J. Chem. Phys. **2008**, 112, 11873

24. A. Weaver, D. W. Arnold, S. E. Bradforth, D. M. Neumark, J. Chem. Phys. **1991**, 94, 1740-1751

25. B. Jagoda-Cwiklik, X. -B. Wang, H. -K. Woo, J. Yang, G. -J. Wang, M. Zhou, P. Jungwirth, L. -S. Wang, J. Phys. Chem. A. **2007**, 111, 7719-7725

26. F. Kita, A. Kawakami, J. Nie, T. Sonoda, H. Kobayashi, J. Power Sources **1997**, 68, 307-310

27. F. Kita, H. Sakata, S. Sinomoto, A. Kawakami, H. Kamizori, T. Sonoda, H. Nagashima, J. Nie, N. V. Pavlenko, Y. L. Yagupolskii, J. Power Sources **2000**, 90, 27-32

28. A. D. Becke, J. Chem. Phys. **1993**, 98, 5648-5652

29. C. L. Lee, W. Yang, R. G. Parr, Phys. Rev. B **1988**, 37, 785-789

30. S. H. Vosko, L. Wilk, M. Nusair, Can. J. Phys. **1980**, 58, 1200-1211

31. M. Ue, A. Murakami, S. Nakamura, J. Electrochem. Soc. **2002**, 149, A1572-A1577

32. R. Krishnan, J. S. Binkley, R. Seeger, J. A. Pople, J. Chem. Phys. **1980**, 72, 650-654

33. O. Borodin, G. D. Smith, J. Phys. Chem. B **2006**, 110, 6293-6299

34. P. Johansson, J. Phys. Chem. A **2006**, 110, 12077-12080

35. P. Johansson, J. Phys. Chem. A **2007**, 111, 1378-1379

36. M. W. Schmidt, K. K. Baldridge, J. A. Boatz, S. T. Elbert, M. S. Gordon, J. J. Jensen, S. Koseki, N. Matsunaga, K. A. Nguyen, S. Su, T. L. Windus, M. Dupuis, J. A. Montgomery Jr., J. Comput. Chem. **1993**, 14, 1347-1363

37. M. S. Gordon, M. W. Schmidt, Advances in Electronic Structure Theory: GAMESS a Decade Later. In Theory and Applications of Computational Chemistry; C. E. Dykstra, G. Frenking, K. S. Kim, G. E. Scuseria, Eds; Elsevier, Amsterdam, The Netherlands, **2005**; chapter 41, pp 1167-1189

38. T. H. Dunning Jr., J. Chem. Phys. **1989**, 90, 1007–1023

39. D. E. Woon, T. H. Dunning Jr., J. Chem. Phys. **1995**, 103, 4572–4585.

40. T. J. Lee, D. Jayatilaka, Chem. Phys. Letters. **1993**, 201, 1-10

41. D. A. Dixon, D. Feller, K. O. Christe, W. W. Wilson, A. Vij, V. Vij, H. D. Brook Jenkins, R. M. Olson, M. S. Gordon, J. Am. Chem. Soc. **2004**, 126, 834-843

42. M. M. Meyer, S. R. Kass, J. Phys. Chem. A **2010**, 114, 4086–4092

43. Y. Takahata, D. P. Chong, Relat. Phenom. **2003**, 133, 69-76

44. L. Wang, T. Maxisch, G. Ceder, Phys. Rev. B **2006**, 73, 195107-195113

45. J. Geith, T. M. Klapotke, J. Weigand, G. Holl, Prop. Exp. Pyro. **2004**, 29, 3-8

46. P. J. Linstrom, W. G. Mallard, NIST Chemistry WebBook

47. S. D. Chambreau, S. Schneider, M. Rosander, T. Hawkins, C. J. Gallegos, M. F. Pastewait, G. L. Vaghjiani, J. Phys. Chem. A **2008**, 112, 7816–7824

48. I. A. Shkrob, T. W. Marin, J. F. Wishart, J. Phys. Chem. B **2013**, 117, 7084−7094

49. M. W. Schmidt, M. S. Gordon, J. A. Boatz, J. Phys. Chem. A, **2005**, 109, 7285-7295

50. K. A. Newton, R. Amunugama, S. A. McLuckey, J. Phys. Chem. A **2005**, 109, 3608-3616

Table 1. Calculated Proton Affinities of Anions in eV

	Without ZPE correction		With ZPE correction			
Anion	CR-CC(2,3)	MP2	CR-CC(2,3)	MP2	Exp.[a]	Previous Theory
N_3^-	15.046	14.657	14.744	14.355	14.808±0.03	
$PH_2O_2^-$	14.659	14.548	14.326	14.215		
NO_3^-	14.382	14.301	14.050	13.969	14.07±0.01	13.81-15.14[b,e,f]
BH_4^-	14.534	14.506	14.221	14.193		
$N(NO_2)_2^-$	13.818	13.777	13.463	13.422	13.183±0.31	13.17-13.598[b,d]
$N(CN)_2^-$	13.650	13.581	13.353	13.284		13.13-13.45[c,d]
BH_3CN^-	13.551	13.439	13.222	13.110		
ClO_4^-	13.319	13.292	13.008	12.981	13.01±0.25	
$BH_2(CN)_2^-$	12.139	12.133	11.914	11.908		

[a] Ref. 46,[b]Ref. 47 B3LYP/6-31+G(d,p), [c]Ref. 48 B3LYP/6-31+G(d,p), [d]Ref. 49 MP2/6-31++G(d,p), [e]Ref. 45 MP2/cc-pVDZ, [f]Ref.504 MP2/6-311+G(2d,2p)

MP2 and CR-CC(2,3) proton affinities calculated using the aug-cc-pVTZ basis set. ZPE calculated from MP2 Hessians.

Table 2. Calculated Ionization Potential in eV using aug-cc-pVTZ basis

anion	CR-CC(2,3)	MP2	exp.	previous theory
N_3^-	2.657	3.091	2.68±0.03[a]	2.64[e]
$PH_2O_2^-$	4.661	5.293		
NO_3^-	4.057	3.423	3.937±0.014[b]	
BH_4^-	4.638	4.692		
$N(NO_2)_2^-$	4.980	5.429		
$N(CN)_2^-$	4.123	4.444	4.135±0.01[c]	
BH_3CN^-	5.506	5.755		
ClO_4^- [f]	5.600	5.661	5.25±0.10[c]	5.19[d]
$BH_2(CN)_2^-$	7.041	7.741		

[a] Ref. 13, [b] Ref. 24, [c] Ref. 46,[d] Ref 42 B3LYP/6-311+G(2df,2pd),
[e] Ref 41 CASPT2/ANO(4s3p2d1f), [f] B3LYP/aug-cc-pVTZ IP = 5.379 eV

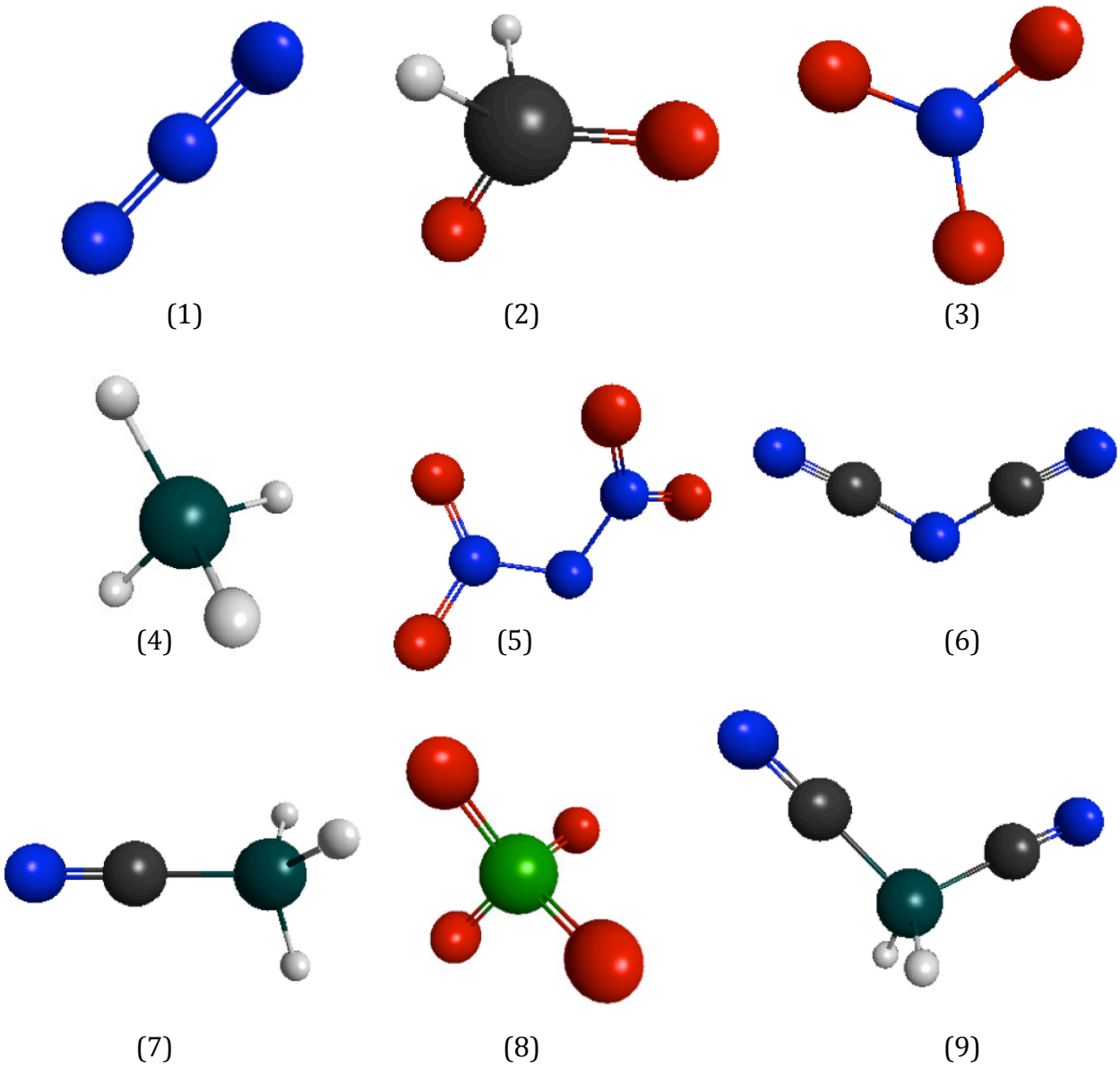

Figure 1. Optimized geometries of the anions presented in this work: 1) azide N_3 2) phosphinate PH_2O_2 3) nitrate NO_3 4) borohydride BH_4 5) dinitramide $N(NO_2)_2$ 6) dicyanamide $N(CN)_2$ 7) cyanoborohydride BH_3CN 8) perchlorate ClO_4 9) dicyanoboride $BH_2(CN)_2$.

CHAPTER 3: AB INITIO INVESTIGATION OF CATION PROTON AFFINITY AND PROTON TRANSFER ENERGY FOR ENERGETIC IONIC LIQUIDS

A paper submitted to be published in the *Journal of Physical Chemistry A*

Caleb Carlin and Mark S. Gordon

Abstract

The protonation of the anion in an ionic liquid plays a key role in the hypergolic reaction between ionic liquids and oxidizers like white fuming nitric acid. To investigate the influence of the cation on the protonation reaction, the deprotonation energy of a set of cations has been calculated at the MP2 level of theory. Specifically, guanidinium, dimethyltriazanium, triethylamine, N-ethyl-N-methyl-pyrrolidinium, N-ethyl-pyridinium, 1,4-dimethyl-1,2,4-triazolium, 1-ethyl-4-methyl-1,2,4-triazolium, and 1-butyl-4-methyl-1,2,4-triazolium were studied. In addition, the net proton transfer energies from the cations to a set of previously studied anions has been calculated, demonstrating an inverse correlation between the net proton transfer energy and the likelihood that the cation/anion combination will react hypergolically with white fuming nitric acid. It is suggested that this correlation occurs due to a balance between the energy released by the proton transfer and the rate of proton transfer as determined by the ionicity of the ionic liquid.

Introduction

Originally reported independently by several researchers around the start of the 1900s, research interest in ionic liquids, salts with melting temperatures below 100 °C, has grown exponentially since the development of customizable ionic liquids based on the pyridinium and imidazolium cations in 1975 and 1982 [1,2]. In addition to the low melting temperatures, ionic liquids exhibit common properties including very low vapor pressures, high thermal stability, and the ability to solvate polar and non-polar molecules[3]. Other properties such as viscosity, conductivity, density, and reactivity can be customized over a wide range of values via the choice of anion and varying the substituents on the cation[4]. The ability to customize drives research into diverse applications such as green solvents in organic synthesis, media for nanostructure formation, electrolytes in batteries, and as energy dense fuels[5].

Research into using ionic liquids for high-energy fuels has identified ionic liquids that spontaneously ignite on contact with strong oxidizers, a process called a hypergolic reaction[6,7]. The ionic liquids that have been determined to react hypergolically either contain nitrogen rich anions that react hypergolically with white fuming nitric acid (WFNA) or boron containing anions that react hypergolically with WFNA and high-test peroxide (HTP)[5,8,9]. However, it is not understood why some ionic liquids react hypergolically and others do not. A previous paper that addressed the mechanism of hypergolic reactions between alkyl-multiamines and inhibited red fuming nitric acids reported that the ignition delay of the amines increases with increasing basicity of the fuel in contradiction to expectations based on energetics[10]. Amine proton affinity as a

measure of basicity does not predict the order of ignition delay of the amine fuels, but does predict the hypergolicity of the amine with WFNA. The present work investigates the deprotonation energy of cations as part of an effort to identify a property of ionic liquids that accurately predicts whether the ionic liquid will react hypergolically with WFNA or HTP independent of relative ignition delay.

The ionic liquids under investigation for hypergolic fuels belong to the subset of protic ionic liquids, formed from the proton transfer from an acid to a base[11]. The ionicity of protic ionic liquids in the condensed phase is not currently understood well enough to predict based on the composition of the ionic liquid alone. High ionicity corresponds to a condensed phase ionic liquid comprised completely or almost completely of ions[12]. The difference in the aqueous pKa of the cation and the anion has been used as a crude metric to predict high ionicity for ionic liquids with a net delta pKa greater than 10, but this measure does not predict a specific value for the ionicity[13,14]. Molecular dynamics simulations have been used to probe the ionicity of ionic liquids that contain large, organic anions such as bis(trifluoromethylsulfonyl)amide (Tf2N), but did not fully reproduce experimental results[15,16]. The ionicities of ionic liquids have been experimentally determined by calculating the product of the effective conductivity and viscosity compared to that of the ideal case of KCl in accordance with the Walden Rule[17]. Experimental measurements of ionicity in ionic liquids employ the Walden Rule, the observation that the product of the specific ion conductivity and the viscosity of a liquid is equal to a temperature dependent constant[17]. The ionicity is determined by plotting the natural log of the conductivity vs. the natural log of the viscosity and comparing the slope of the line created to the slope of the ideal case of KCl. An improvement on the Walden

Rule based on the Nernst-Einstein equation takes into account the size of the ions in the liquid and has been shown to provide more accurate results[12]. An experimental study of N-methylpyrrolidine with acetic acid and dimeric acetic acid chains shows an increase in the ionicity of the ionic liquid as the concentration of dimeric acetic acid (proton affinity 6.99 eV) increases relative to that of acetic acid (proton affinity 8.54 eV)[13]. A comparison of the measured ionicities of lithium-triglyme based ionic liquids for the anions trifluoroacetate, nitrate, triflate, borotetrafluoride, perchlorate, and Tf2N with the gas phase proton affinity of each anion shows a general correlation between increasing proton affinity and decreasing ionicity, although there are exceptions to the trend for anions that have similar proton affinities[18]. Less is known about the role that the cation plays in determining the ionicity of ionic liquids. Experimental measurements have shown no correlation between the size of the cation and the viscosity of the ionic liquid, though varying the alkyl chain length and the composition of the substituents does impact the ionicity and viscosity[12,16].

The exact reaction pathway of the hypergolic reaction for protic ionic liquids is not known, however the evidence indicates that the protonation of the anion plays a key role in determining which ionic liquids react hypergolically. The standard test for a hypergolic reaction involves releasing a droplet of fuel into a cuvette containing the oxidizer as represented in Figure 1[19]. High-speed photography of the drop test of 1-ethyl-3-methyl-imidazolium dicyanamide and WFNA has shown that following the contact between the oxidizer and ionic liquid, a vigorous reaction in the condensed phase ejects droplets into the vapor phase where the ignition occurs. The exothermic transfer of the proton from the acid to the dicyanamide has been identified as the first step in the

hypergolic reaction[7]. Repeating the drop test with sodium dicyanamide confirms that the proton transfer occurs between the acid and the anion[20]. Based on the experiments on dicyanamide based ionic liquids, it is anticipated that the proton affinity of the anion is the dominant factor in determining how much energy is released during the proton transfer step of the reaction. In contrast, the ionicity of an ionic liquid is dependent on both the anion and cation. One therefore might expect that the difference between the proton affinities of the anion and the conjugate base of the cation would provide a more accurate method of predicting ionicities than just the proton affinity of the anion alone. Analysis of the droplets in the vapor phase by Fourier transform infrared spectroscopy shows no presence of the protonated dicyanamide, evidence that the reaction progresses beyond the proton transfer step entirely in the condensed phase[19]. Due to the rapid and vigorous nature of the start of the hypergolic reaction, computational methods provide an effective way to probe the reaction prior to the formation of the vapor phase.

Because of the considerable variety of combinations that result from varying the substituents on the cation, the subset of cations for which experimental proton affinities are available is small. Of the cations in the present study, only the unsubstituted guanidine and triethylamine have previously reported experimental or computed proton affinities to use for comparison. The compendium work of Hunter and Lias used a combination of relative ordering of gas phase basicity and a known proton affinity of a representative molecule to predict the proton affinity of other organic molecules[21]. During the mid-1970s, two measurements of the proton affinity of triethylamine using ion cyclotron resonance spectroscopy were reported; the difference between the two values is 5.49 kcal/mol[22,23]. The proton affinity of guanidine was calculated by a

combination method in which the optimized geometry and zero point energies (ZPE) were calculated using Hartree-Fock (HF) and a small basis set, 6-31G(d). Then, the total energy at the optimized geometry was calculated using Møller-Plesset second order perturbation (MP2)[24] theory with a larger basis set, 6-311+G(d,p)[25]. This multilevel approach is similar to the method used in the present study with the exception that a single basis set is used throughout.

In previous work by the present authors, the ionization potential and proton affinity of anions of interest in developing hypergolic ionic liquid fuels were calculated[26]. The results show a general inverse correlation between anion proton affinity and ionization potential, with three exceptions. Nitrate and dicyanamide have ionization potentials that are less than would be predicted by the trend and phosphinate has an ionization potential that is greater than would be predicted by the trend. It was also concluded that MP2 proton affinities are similar to those predicted by the coupled cluster methods CCSD(T)[27] and CR-CC(2,3)[28,29]. Maksic and Kovacevic showed that calculating the change in total energy using MP2 and applying the ZPE correction from frequencies calculated at the Hartree-Fock level of theory can accurately reproduce experimental proton affinities of large systems[25]. The present work complements the previously published anion results[26] by calculating the deprotonation energy of cations that form energetic ionic liquids with the previously studied anions.

Methods

All calculations were completed with the GAMESS software package[30,31] using the augmented correlation consistent triple zeta (aug-cc-pVTZ) basis set[32,33]. Optimized

geometries for all cations and neutral molecules were calculated at the HF and MP2 levels of theory. To determine the lowest energy deprotonation energy for the cations, the process was repeated for each symmetrically distinct proton on the cation. To confirm that optimized geometries are minima, the analytic Hessian was calculated and diagonalized for all final HF geometries, and the HF and MP2 geometries were compared. The zero point energy calculated from the HF Hessian is included in the calculation so that the deprotonation energy is given by equation 1.

$$E_{DP} = E_C^{MP2} - E_{HC^+}^{MP2} + (E_{ZPE,C}^{HF} - E_{ZPE,HC^+}^{HF}) \quad (1)$$

The net reaction energies of the proton transfer reaction were calculated by finding the difference in changes in energy based on equation 2, in which A is the anion,

$$\begin{aligned} HC^+ &\longrightarrow C + H^+ \\ H^+ + A^- &\longrightarrow HA \end{aligned} \quad (2)$$

C is the deprotonated cation, and H is the proton. Proton affinities of the anions were taken from previous MP2/aug-cc-pVTZ calculations[26].

Results and Discussion

The cations, chosen for this study are (See Figure 2) guanidinium (Guan), dimethyltriazanium (DMT), triethylamine (TEA), 1-ethyl-1-methylpyrrolidinium (EMPyrr), 1-ethylpyridinium (EPyr), 1,4-dimethyl-1,2,4-triazolium (MMTZ), 1-ethyl-4-methyl-1,2,4-triazolium (EMTZ), and 1-butyl-4-methyl-1,2,4-triazolium (BMTZ). Table 1 compares the calculated HF and MP2 deprotonation energies in eV, along with the available reported experimental deprotonation energies. For each cation, the location of

the proton that has the smallest deprotonation energy (SDE) is given in the column labeled "Position" in Table 1. For triethylamine and guanidinium, the average absolute difference in deprotonation energy between the previously reported values and the MP2 energies, 0.119 eV and 0.064 eV respectively, is considerably less than the average absolute difference for HF, 0.217 eV and 0.342 eV respectively, as expected. In all cases the SDE position is the same for HF and MP2, except in the case of 1-ethylpyridinium.

The net proton transfer (NPT) energies from cation to anion are presented in Table 2 using the MP2 cation deprotonation energies in Table 1 and the anion proton affinities in Table 3[26]. The columns in Table 2 are arranged in order of decreasing proton affinity from left to right. The NPT energies also decrease from left to right in accordance with equation 2. The average NPT energy for each anion, determined by averaging the NPT energy of all combinations of the anion with the cations included in this work, is given in the last row in Table 2. Of the four anions with the smallest average NPT energy, dicyanamide and dicyanoborohydride have been shown to react hypergolically with WFNA for a wide range of cations[5]. Cyanoborohydride has also been shown to react hypergolically with WFNA for some cations, but is not as thoroughly tested because the ionic liquids are hygroscopic[34]. Of the four anions with the largest average NPT energy, azide, phosphinate, and nitrate form ionic liquids that either do not react hypergolically or exhibit very long ignition delays[6]. This result matches the positive correlation demonstrated for monomolecular fuels by McQuaid that ignition delays increase in direct proportion with the proton affinity, including a lack of ignition for the largest proton affinities[10].

Conventional understanding might predict that the more energy released by the protonation of the anion, the more total energy that is available to drive the hypergolic reaction to a faster ignition. Such a conclusion, however, disagrees with multiple studies, including the present work. A resolution of this apparent contradiction is suggested by the nature of ionic liquids. Ionic liquids as a class of compounds are characterized by smaller ion-ion interactions than traditional salts and greater intermolecular interactions than neutral organic mixtures. Ionic liquids, then, are in an interaction energy "sweet spot" in that they behave neither like a traditional high-temperature melting salt nor like an organic liquid composed of neutral molecules. Therefore, it is suggested that ionic liquids that react hypergolically have a NPT energy and ionicity that maximize the total energy released in the early steps of the reaction, instead of maximizing the energy released in each individual proton transfer. If one interprets the ionicity as a measure of the fraction of the bulk ionic liquid that exists as ions at equilibrium, an ionic liquid with low ionicity has fewer anions available for proton transfer than does an ionic liquid with high ionicity. An ionic liquid with a very large NPT energy and low ionicity releases an insufficient amount of energy in a short enough time to facilitate the hypergolic reaction, because the rate of proton transfers to the anions is too low due to the low concentration of anions in the ionic liquid. An ionic liquid with a very small NPT energy and high ionicity similarly fails to release enough energy to facilitate the hypergolic reaction, because the rate of proton transfers is high but the energy released by each proton transfer is too small. Thus, ionic liquids that react hypergolically should have NPT energies and ionicities that fall within a range of values such that the rate of proton transfers multiplied by the energy released by each proton transfer is sufficient to facilitate the hypergolic

reaction. None of the ionic liquids included in the present work represent the case for which the NPT energy is too small. Examples of ionic liquids (e.g., N-methylpyrrolidinium acetate) have been reported in the literature[13] that do not react hypergolically, *and* have NPT energy values that are much lower than those of the ionic liquids in the present study. Perchlorate provides an exception to the proposed explanation, because the perchlorate average NPT energy of -2.17 eV lies between those of dicyanamide (-2.47 eV) and dicyanoborohydride (-1.10 eV), but does not readily form ionic liquids that react hypergolically. Thus it is concluded that for an ionic liquid to react hypergolically, it is necessary but not sufficient to have a NPT energy and ionicity within a specific range of values such that the proton transfer to the anion releases enough energy at a fast enough rate to facilitate the hypergolic reaction.

Future work to confirm the conclusion in this paper will rely on increasing the available experimental data regarding the sets of ionic liquids for which the NPT energy, the ionicity, and hypergolic reactivity with WFNA are known. At present, the observed trend between proton affinity, NPT energy, and hypergolic reactivity appears to be general, but might only apply to the subset of ionic liquids represented in the present study. However, a very recent paper by Vogl and co-workers, published[35] while the present work was under review, demonstrates the importance of the cation and the cation structure in determining properties of protic ionic liquids. Of course, it is possible that the proton equilibrium constant analogous to the pKa but determined in the anhydrous ionic liquid environment will be a more accurate predictor of ionicity than the proton affinity of the anion or the NPT energy. The reason this may be the case is that the NPT energy

is a gas phase property and does not include the intermolecular interactions that are present in the liquid phase where the proton transfer occurs.

Conclusion

In this paper, the calculated deprotonation energies of selected ionic liquid cations of interest are presented as well as the net energies for the proton transfer reaction between the cations in the present work and anions that were previously studied. The deprotonation energies show little variance, with slightly higher energies for the cations with cyclic structures. Ordering the ionic liquids investigated by decreasing average NPT energy illustrates a separation between ionic liquids that have large NPT energies and do not react hypergolically and ionic liquids that have small NPT energies and do react hypergolically. It is proposed that the trend in NPT energies and reactivity is determined by the need to balance ion concentration in the ionic liquid and the energy released by the protonation of the anion. This suggestion is supported by the recent paper by Vogl etal.[35]

Acknowledgements.

This material is based upon work supported by the Air Force Office of Scientific Research under AFOSR Award No. FA9550-14-1-0306. This work was supported in part by a grant of computer time from the DoD High Performance Computing Modernization Program at the Air Force Research Laboratory DoD Supercomputing Resource Center. The authors thank Dr. Jerry Boatz for his critical reading of this manuscript.

References

1) Chum, H. L.; Koch, V. R.; Miller, L. L.; Osteryoung, R. A. Electrochemical Scrutiny of Organometallic Iron Complexes and Hexamethylbenzene in a Room Temperature Molten Salt. J. Am. Chem. Soc. 1975, 97, 3264-3265.

2) Wilkes, J. S.; Levisky, J. A.; Wilson, R. A.; Hussey, C. L. Dialkylimidazolium Chloroaluminate Melts: A New Class of Room-Temperature Ionic Liquids for Electrochemistry, Spectroscopy and Synthesis. Inorg. Chem. 1982, 21, 1263-1264.

3) Zhang, S.; Sun, N.; He, X.; Lu, X.; Zhang, X. Physical Properties of Ionic Liquids: Database and Evaluation. J. Phys. Chem. Ref. Data 2006, 35, 1475-1517.

4) Canongia Lopes, J. N.; Costa, M. F.; Pádua, A. A. H. Nonpolar, Polar, and Associating Solutes in Ionic Liquids. J. Phys. Chem. B. 2006, 110, 16816-16818.

5) Zhang, Y.; Gao, H. X.; Joo, Y. -H.; Shreeve, J. M. Ionic Liquids as Hypergolic Fuels. Angew. Chem. Int. Ed. 2011, 50, 9554-9462.

6) Schneider, S.; Hawkins, T.; Rosander, M.; Vaghjiani, G.; Chambreau, S.; Drake, G. Ionic Liquids as Hypergolic Fuels. Energy Fuels 2008, 22, 2871-2872.

7) Chambreau, S. D.; Schneider, S.; Rosander, M.; Hawkins, T.; Gallegos, C. J.; Pastewait, M. F.; Vaghjiani, G. L. Fourier Transform Infrared Studies in Hypergolic Ignition of Ionic Liquids. J. Phys. Chem. A 2008, 112, 7816-7824.

8) Gao, H.; Shreeve, J. M. Azole-Based Energetic Salts. Chem. Rev. 2011, 111, 7377-7436.

9) Schneider, S.; Hawkins, T.; Ahmed, Y.; Rosander, M.; Hudgens, L.; Mills, J. Green Bipropellants: Hydrogen-Rich Ionic Liquids that are Hypergolic with Hydrogen Peroxide. Angew. Chem. Int. Ed. 2011, 123, 6008-6010.

10) McQuaid, M. J. Computationally Based Measures of Amine Azide Basicity and Their Correlation With Hypergolic Ignition Delays. ARL-TR-3122; U.S. Army Research Laboratory: Aberdeen Proving Ground, MD, December 2003.

11) Greaves, T. L.; Drummond, C. J. Protic Ionic Liquids: Properties and Applications. Chem. Rev. 2008, 108, 206-237.

12) MacFarlane, D. R.; Forsyth, M.; Izgorodina, E. I.; Abbott, A. P.; Annat, G.; Fraser, K. On the Concept of Ionicity in Ionic Liquids. Phys. Chem. Chem. Phys. 2009, 11, 4962-4967.

13) Johansson, K. M.; Izgorodina, E. I.; Forsyth, M.; MacFarlane, D. R.; Seddon, K. R. Protic Ionic Liquids Based on the Dimeric and Oligomeric Anions: $[(AcO)_xH_{x-1}]^-$. Phys. Chem. Chem. Phys. 2008, 10, 2972-2978.

14) Stoimenovski, J.; Izgorodine, E. I.; MacFarlane, D. R. Ionicity and Proton Transfer in Protic Ionic Liquids. Phys. Chem. Chem. Phys. 2010, 12, 10341-10347.

15) Liu, H.; Maginn, E. An MD Study of the Applicability of the Walden Rule and the Nernst-Einstein Model for Ionic Liquids. ChemPhysChem 2012, 13, 1701-1707.

16) Zhang, Y.; Maginn, E. J. Direct Correlation Between Ionic Liquid Transport Properties and Ion Pair Lifetimes: A Molecular Dynamics Study. J. Phys. Chem. Lett. 2015, 6, 700-705.

17) Schreiner, C.; Zugmann, S.; Harti, R.; Gores, H. J. Fractional Walden Rule for Ionic Liquids: Examples from Recent Measurements and a Critique of the So-Called Ideal KCl Line for the Walden Plot. J. Chem. Eng. Data 2010, 55, 1784-1788.

18) Mandai, T.; Yoshida, K.; Ueno, K.; Dokko, K.; Watanabe, M. Criteria for Solvate Ionic Liquids. Phys. Chem. Chem. Phys. 2014, 16, 8761-8772.

19) Chowdhury, A.; Thynell, S. T.; Wang, S. Ignition Behavior of Novel Hypergolic Materials. AIAA/ASME/SAE/ASEE Joint Propulsion Conference & Exhibit, 2009, 1.

20) Litzinger, T.; Iyer, S. Hypergolic Reaction of Dicyanamide-Based Fuels with Nitric Acid. Energy Fuels 2011, 25, 72-76.

21) Hunter, E. P. L.; Lias, S. G. Evaluated Gas Phase Basicities and Proton Affinities of Molecules: an Update. J. Phys. Chem. Ref. Data 1998, 27, 413.

22) Arnett, E. M.; Mitchell, E. J.; Murty, T. S. S. R. Basicity. Comparison of Hydrogen Bonding and Proton Transfer to Some Lewis Bases. J. Am. Chem. Soc., 1974, 96, 3875-3891.

23) Aue, D. H.; Webb, H. M.; Bowers, M. T. Quantitative Proton Affinities, Ionization Potentials, and Hydrogen Affinities of Alkylamines. J. Am. Chem. Soc. 1976, 98, 311-317.

24) Moller, C.; Plesset, M. S. Note on an Approximation Treatment for Many-Electron Systems. Phys. Rev. 1934, 46, 618-621.

25) Maksic, Z. B.; Kovacevic, B. Absolute Proton Affinity of Some Polyguanides. J. Org. Chem. 2000, 65, 3303-3309.

26) Carlin, C.; Gordon, M. S. Ab Initio Calculation of Anion Proton Affinity and Ionization Potential for Energetic Ionic Liquids. J. Comput. Chem. 2015, 36, 597-600.

27) Raghavachari, K.; Trucks, G. W.; Pople, J. A.; Head-Gordon, M. A Fifth-Order Perturbation Comparision of Electron Correlation Theories. Chem. Phys. Lett. 1989, 157, 479-483.

28) Kowalski, K.; Piecuch, P. New Coupled-Cluster Methods with Singles, Doubles, and Noniterative Triples for High Accuracy Calculations of Excited Electronic States. J. Chem. Phys. 2004, 120, 1715-1738.

29) Izgorodina, E. I; Forsyth, M.; MacFarlane, D. R. Towards a Better Understanding of 'Delocalized Charge' in Ionic Liquid Anions. Aust. J. Chem. 2007, 60, 15-20.

30) Schmidt, M. W.; Baldridge, K. K.; Boatz, J. A.; Elbert, S. T.; Gordon, M. S.; Jensen, J. J.; Koseki, S.; Matsunaga, N.; Nguyen, K. A.; Su, S.; Windus, T. L.; Dupuis, M.; Montgomery, J. A. Jr. General Atomic and Molecular Electronic Structure System. J. Comput. Chem. 1993, 14, 1347-1363.

31) Gordon, M. S.; Schmidt, M. W. Advances in Electronic Structure Theory: GAMESS a Decade Later. In Theory and Applications of Computational Chemistry; Dykstra, C. E.; Frenking, G.; Kim, K. S.; Scuseria, G. E. Eds; Elsevier, Amsterdam, The Netherlands, 2005; chapter 41, pp 1167-1189

32) Dunning, T. H. Jr. Gaussian Basis Sets for Use in Correlated Molecular Calculations. I. The Atoms Boron Through Neon and Hydrogen. J. Chem. Phys. 1989, 90, 1007-1023.

33) Woon, D. E.; Dunning, T. H. Jr. Gaussian Basis Sets for Use in Correlated Molecular Calculations. V. Core-Valence Basis Sets for Boron Through Neon. J. Chem. Phys. 1995, 103, 4572-4585.

34) Schneider, S.; Hawkins, T.; Ahmed, Y.; Rosander, M.; Hudgens, L.; Mills, J. Green Bipropellants: Hydrogen-Rich Ionic Liquids That are Hypergolic with Hydrogen Peroxide. Angew. Chem. Int. Ed. 2011, 50, 5886-5888.

35) Vogl, T.; Goodrich, P.; Jacquemin, J.; Passerini, S.; Balducci, A. The Influence of Cation Structure on the Chemical−Physical Properties of Protic Ionic Liquids. J. Phys. Chem. C. 2016, preprint

Table 1: Calculated Deprotonation Energies in eV

Cation	HF	MP2	Reported Values	Position[f]
DMT	11.463	10.932		A1
TEA	10.31	10.012	9.974-10.212[a,b,c]	N1
EMPyrr	13.03	11.849		M1
Epyr	11.943	11.282		2/E1[e]
Guan	10.519	10.113	10.134,10.22[a,d]	A1
MMTZ	10.883	10.715		5
EMTZ	10.961	10.786		5
BMTZ	10.969	10.791		5

[a]Ref. 21, [b]Ref. 22, [c]Ref. 23, [d]Ref. 25, [e]position is for HF/MP2 deprotonation energy, [f]location of proton removed as labeled in figure 2.

Table 2: Net energy change of proton transfer reaction in eV

	N_3^-	$PH_2O_2^-$	BH_4^-	NO_3^-	$N(NO_2)_2^-$	$N(CN)_2^-$	BH_3CN^-	ClO_4^-	$BH_2(CN)_2^-$
DMT	-3.42	-3.28	-3.26	-3.04	-2.49	-2.35	-2.18	-2.05	-0.98
TEA	-4.34	-4.20	-4.18	-3.96	-3.41	-3.27	-3.10	-2.97	-1.90
EMPyrr	-2.51	-2.37	-2.34	-2.12	-1.57	-1.44	-1.26	-1.13	-0.06
EPyr	-3.07	-2.93	-2.91	-2.69	-2.14	-2.00	-1.83	-1.70	-0.63
Guan	-4.24	-4.10	-4.08	-3.86	-3.31	-3.17	-3.00	-2.87	-1.80
MMTZ	-3.64	-3.50	-3.48	-3.25	-2.71	-2.57	-2.40	-2.27	-1.19
EMTZ	-3.57	-3.43	-3.41	-3.18	-2.64	-2.50	-2.32	-2.20	-1.12
BMTZ	-3.56	-3.42	-3.40	-3.18	-2.63	-2.49	-2.32	-2.19	-1.12
Average	-3.55	-3.41	-3.38	-3.16	-2.61	-2.47	-2.30	-2.17	-1.10

Table 3. Calculated Proton Affinities of Anions in eV[26]

Anion	MP2
N_3^-	14.355
$PH_2O_2^-$	14.215
BH_4^-	14.193
NO_3^-	13.969
$N(NO_2)_2^-$	13.422
$N(CN)_2^-$	13.284
BH_3CN^-	13.110
ClO_4^-	12.981
$BH_2(CN)_2^-$	11.908

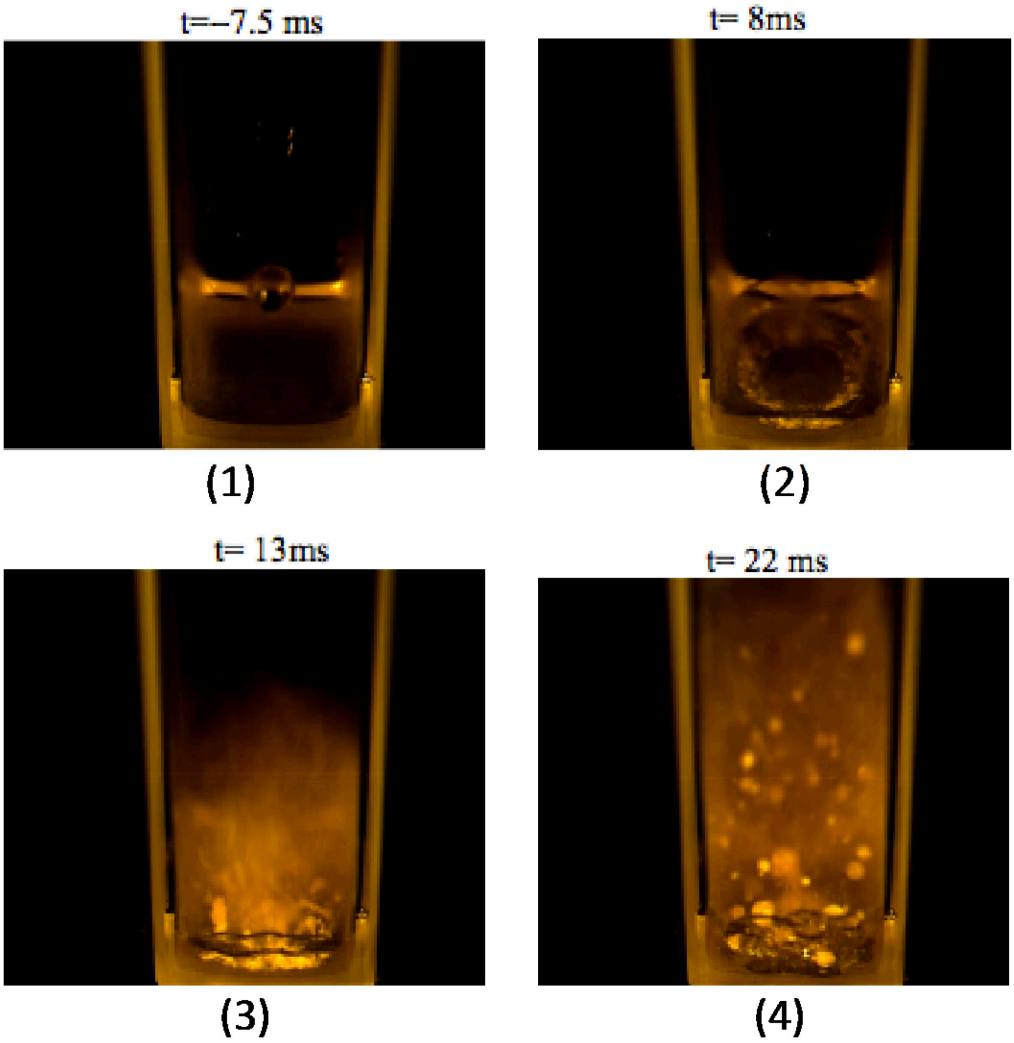

Figure 1. Select images of hypergolic reaction of ethyl-methyl-imidazolium dicyanamide and WFNA. (1) Droplet of fuel released above WFNA. (2) Vigorous reaction occurs at fuel/oxidizer interface, generating vortices in the oxidizer. Proton transfer to dicyanamide occurs here. (3) Aerosolized droplets are ejected into the vapor phase. (4) Ignition occurs in the vapor phase. Images taken from reference 19.

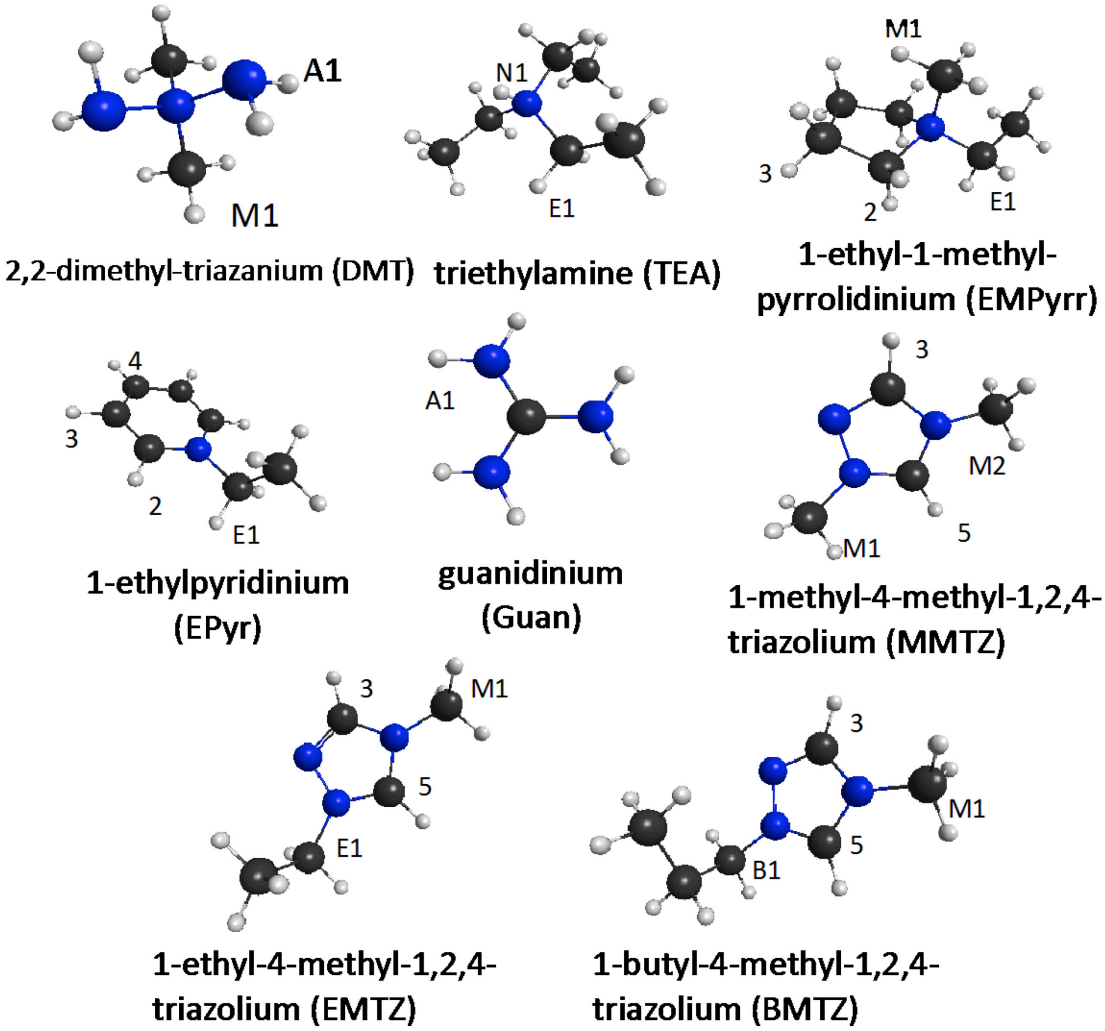

Figure 2. Optimized geometries of cations presented in this work. Labels denote the symmetrically distinct protons that were tested to determine the lowest deprotonation energy for each cation.

CHAPTER 4: FULLY QUANTUM MECHANICAL MONTE CARLO METHOD

A paper to be submitted to the *Journal of Computational Chemistry*

Caleb Carlin and Mark S. Gordon

Abstract

A Metropolis Monte Carlo (MMC) method that completely incorporates quantum mechanical (QM) methods is presented. The QM/MMC method supports fully ab initio methods as well as the fragment molecular orbital and effective fragment potential methods. Support for preserving chemical bonds between Monte Carlo groups and internal flexibility within Monte Carlo groups is included, with the introduction of pair binding and a secondary Monte Carlo implementation. The QM/MMC method was applied to locating the minimum energy structures of five methanol clusters and the minimum energy structure of n-octadecane, a large molecule that was internally fragmented.

Introduction

Nearly seven decades after the introduction of the Monte Carlo Method (MC)[1], the method remains an important tool in studying complex systems to determine global or low lying minima on potential energy surfaces and for use with methods for which analytic gradients are not available. Based on the older and broader technique of statistical sampling, the MC method introduces formalism for randomly sampling a system so that the set of data points sampled has a known distribution2. The development and application of the MC method to ever more complex and larger systems has paralleled the development of faster computers capable of performing the nearly countless calculations required. Far from the first calculations of neutrino interactions on

the analog computer FERMIAC[2], today fully ab initio quantum mechanical (QM) calculations are commonplace and should be suitable for use with MC simulations.

Central to the use of MC methods in chemistry is the Metropolis Monte Carlo (MMC) method and the use of Markov Chains. The Markov Chain stochastic model describes systems for which the state at any given point is dependent only on the previous state of the system. For MMC, each sampled data point or step is determined by perturbing the state of the previously sampled data point[3,4]. Unlike other MC methods in which the value of each sample is weighted to match an intended distribution, in the MMC approach the probability of accepting or rejecting each new data point is weighted based on the property being minimized, generally the energy, between the current and previous data points. The set of data points is a distribution based on the choice of weighting. The most common choice of weighting for chemistry applications is the Boltzmann factor[5].

Most classical MMC simulations are performed with generalized classical force fields like AMBER[6-10], OPLS[11-14], and CHARMM[15-17] that are implemented in software packages including AMOEBA[18-19], TINKER[18], BOSS[19], Cassandra[20], and RASPA[21]. Efforts to extend MMC beyond classical potentials have included hybrid combinations of classical and quantum calculations[22-23], semi-empirical methods[24-25], and efficient course grained potentials[26]. The effective fragment potential (EFP) method[27], a sophisticated model potential derived directly from quantum mechanics, has also used the MMC method successfully to obtain local and global minima for liquids and liquid mixtures[28,29]. The EFP method, implemented in GAMESS, is a semi-classical model based on quantum mechanics (QM), with no empirically fitted parameters, that was

designed to examine intermolecular interactions, including solvent effects[27,30-32]. The EFP method has been applied successfully to a wide range of problems, including the solvation of ions[33,34], the interactions of nucleotide base pairs[35], and water-alcohol[28,29,36] mixing.

To date, few fully QM MMC implementations, and no entirely ab initio implementations to the authors' knowledge, have been reported. Notably, the dynamic nucleation theory Monte Carlo (DNTMC)[37] method does employ quantum mechanics via a fragmentation approach. Computer capabilities have increased and methods have been developed to reduce computational costs such that a fully ab initio MMC method, as well as a fragmentation method, is viable, as presented in this work. The fragment molecular orbital (FMO) method, also implemented in GAMESS, is designed to study large molecular systems, like proteins and liquids, with accurate electronic structure methods. The FMO method[38,39] divides a molecule into fragments (monomers) in a manner that allows the calculations of each fragment to be performed on a separate node or group of nodes, thereby making the method highly parallel[40]. In the FMO method the electron density of each monomer is obtained iteratively within either the Hartree-Fock (HF) or density functional theory (DFT) approach. The monomer electron density can then be used to calculate monomer-monomer (dimer) or trimer interactions or monomer-EFP interactions, as well as to add electron correlation to a HF calculation. If explicit dimer (trimer) interactions are included, the method is called FMO2 (FMO3). In this paper, molecular species that are treated by fully ab initio methods (i.e., not FMO or EFP) are described as fully ab initio (FAB). Subsets of FAB molecules are called groups here to distinguish them from FMO or EFP fragments. A set of atoms that are collectively

perturbed during a single step of the Monte Carlo search will be referred to as a unit, whether it is an EFP or FMO fragment or an FAB group.

In the previous implementation of MMC in GAMESS,[41] each step in the Markov Chain permitted only movement of the (internally rigid) EFP units. Except for full geometry optimizations at various stages of the simulation, QM units were held fixed or at most limited to short perturbations of each QM atom as part of an EFP translation step. The translation and rotation of EFPs in an MMC simulation were separated into different steps so that no single step included both translations and rotations. The separation of translations and rotations has been shown to decrease the number of steps necessary to locate minima on the potential energy surface[42,43]. All changes in the MMC portion of GAMESS have been made to maintain backward compatibility with previous versions of the program.

In this work the capabilities and limitations of the new method are presented in the context of two test cases. MMC with simulated annealing is used to locate minima of a five-methanol cluster using the EFP, FMO, and FAB methods to compare the computational cost and accuracy of each method. To test the application of MMC to large, internally fragmented molecules, an MMC search is performed on n-octadecane starting from the all-trans conformation.

A cluster of five methanol molecules provides a second useful test case for the MMC method. Previous second order perturbation theory (MP2), DFT and classical force field studies of the methanol pentamer have predicted that the global minimum is a five member ring that involves hydrogen bonding of the five OH groups[44-46]. Other minima

that incorporate three and four member rings with branching methanols have also been identified.

Studies of long chain alkanes have determined that as the number of carbon atoms in the chain increases, the lowest energy conformation changes from the all-trans conformation to a folded conformation. The transition between the two types of conformers occurs in the gas phase at n-octadecane (OD), which adopts a global minimum energy conformation that is neither fully extended nor tightly folded[41-43]. A combined experimental and theoretical study of OD using jet spray Raman spectroscopy and a systematic variation of torsional angles to determine minima confirms the transitional nature of OD in that neither the straight chain nor hairpin folded conformers are minima[47]. A configurational-biased Monte Carlo study of OD in water and acetonitrile using a united-atom force field found that OD has an average end-to-end distance of 17 Å, compared to an end-to-end distance of 21 Å that would be expected for the all-trans conformation[48]. An investigation of OD in the gas phase and solvated in water found minimal differences between the free energy surface of the isolated and solvated ODs, suggesting that the results of solvated OD are applicable for gas phase OD[49]. The partial folding of OD in the gas phase is a good test case for MMC, as it is a large molecule with internal flexibility.

Fully QM Monte Carlo

The MMC implementation fully incorporates QM atoms, EFP fragments, and combinations thereof in all aspects of the MMC method (QM/MMC) with support for DFT, HF, and post HF methods. For multi-reference methods, one must use care to be

sure that active spaces are consistent across the swath of a potential energy surface sampled during a QM/MMC simulation.

Incorporating FAB and FMO into the MMC method facilitates the study of chemical systems that have been considered to be too expensive to treat with QM methods that necessitate the calculation of gradients, and sometimes Hessian matrices. The QM/MMC method introduces the possibility to model macromolecules by creating fragment subsystems, each of which can be calculated nearly independently of the others. Internally fragmented molecules have bonds connecting the fragments that must be maintained during the course of the MMC search. Processes like molecular dynamics simulations and geometry optimizations move the atoms based on the gradient of the potential energy, ensuring that movements that break bonds in a non-physical way are excluded. Movements in MMC searches are independent of the potential energy surface, and there is no expectation that two units that are chemically bonded to each other will remain so during the course of the QM/MMC search, unless the bond energy is large enough that any step that breaks the bond is guaranteed to be rejected based on the temperature of the system. To address the issue of non-physical bond breaking, an option, called 'pair binding', has been implemented to limit the absolute distance between pairs of atoms of different FMO or FAB units. Pair binding is a constraint placed on two atoms in different units (e.g., fragments), such that any MMC step in which the two atoms are separated by an absolute difference that is greater than the cut-off is rejected. In this way the chemical bonding structure is maintained while imposing a minimal constraint on the possible configurations of the units.

Pair binding modifies the MMC method in three ways: the *separation* test, the locus of *rotation*, and the *propagation* of movement. The *separation* test occurs following each translation step involving a pair bound unit and before the energy of the system is calculated. The distance between the two pair bound atoms is calculated, and if the distance is greater than the specified cut-off, then the MMC step is rejected. The default cut-off distance is 105% of the sum of the covalent radii of the pair bound atoms. Ordinarily, a *rotation* is centered on the coordinate center of the moving unit. For pair bound units, all rotations are centered on one of the pair bound atoms in the unit that is to be moved in an MMC step. The *propagation* of movement occurs when three or more units are pair bound together to form a network of pair bound units. To illustrate, consider an example system (Figure 1) of four units labeled A, B, C, and D, such that B is pair bound to A, C, and D through the atoms B_A, B_C, and B_D, respectively. If B is selected to be moved as part of an MMC step, then one of the atoms (B_A, B_C, or B_D) is randomly chosen to be the anchor atom; B_A is chosen in Figure 1. For a translation, the movement is applied to B and the separation test occurs between B and the unit pair bound to the anchor atom (A). If the move passes the separation test, the translation is applied to all units in the network that are pair bound to B, either directly or indirectly, except those connected through the anchor atom. The translation is applied along each branch of the network until a terminal unit is reached, and the process continues from the most recent branching point. The result in the example case is that B, C, and D all undergo the same translation and A does not move. For a rotation, the anchor atom is the locus of rotation and the movement is propagated in the same way as for a translation. Thus B, C, and D are rotated by the same angle around B_A, and A again remains

unmoved. While designed for modeling large molecules that are internally divided into FMO fragments, the pair binding option works with FMO and FAB units and can be applied to the challenge of introducing internal flexibility of groups into the MMC search.

Movements in the MMC method are limited to moving rigid units, thus excluding internal relaxation from the phase space of configurations to be sampled. To introduce internal relaxation into the process, two options are implemented in the QM/MMC method: the secondary Monte Carlo search (SMC) and fragmentation of FAB groups with pair binding. As diagrammed in Figure 2, the SMC search occurs during the MMC simulation, between the movement step and the energy calculation step. Holding the rest of the system immobile, the atoms within the unit that is being moved are translated one at a time by a default maximum displacement of 0.6 Å. If the unit being moved is pair bound to another unit, then the pair bound constraint is applied after all SMC steps. After each atom is moved, the total energy of the entire system is calculated and the translation of the atom is accepted or rejected by the normal MMC process. This process is repeated the number of times specified by the user; then, the lowest energy configuration of the unit is used to determine whether to accept or reject the new configuration as part of the main MMC search. There are two factors that potentially limit the utility of applying the SMC method. First, since each step of the SMC search requires calculating the total energy of the system, the number of energy calculations for an MMC search with SMC is the number of MMC steps times the number of steps in each SMC. Therefore, even a modest number of SMC steps can increase the total cost of the simulation by an order of magnitude. To address this, a cut-off temperature can be

specified below which an SMC search is initiated. Second, since the coordinates that are generated at the end of an SMC step correspond to the lowest energy configuration located during the SMC step, a bias would be introduced into the probability distribution of states if those coordinates are used. Then, the set of accepted steps would no longer form a statistically valid ensemble. Therefore, if an SMC search is used, one must employ the option of using the last accepted configuration from the SMC, not the lowest energy configuration.

Another way to introduce internal flexibility into a unit in the QM/MMC method is to combine the pair binding option with careful fragmentation of the FAB molecules. As the choice of how to group a molecule into FAB groups does not affect the calculation of the total energy, the choice of grouping is arbitrary. Assigning each atom to a separate group corresponds to full degrees of internal flexibility. Alternatively, the choice of grouping can be such that only the degrees of internal flexibility of interest are permitted by setting the portions of the molecule that are allowed to move with respect to each other into different groups. The approach of internal flexibility by constrained internal fragmentation can also be done using the FMO method, but care should be taken because electrons in a fragmented molecule are assigned and confined to a fragment in the FMO method, which may result in the electrons being artificially localized in the molecule. The cost scaling of fully ab initio methods provides a practical limit on the size of the system that can be studied with this method. In addition, the number of steps in the QM/MMC search needs to be increased in proportion to the increase in degrees of freedom that results from the introduction of internal flexibility.

Computational Methods

Methanol clusters

The following steps were completed on the methanol cluster using the EFP, FMO, and FAB methods with the GAMESS software package[50,51]. FMO and FAB energies were calculated at the HF/6-31+G(d,p) level of theory. Each MMC unit consisted of a single methanol molecule that was held internally rigid. A single temperature MMC search was carried out for 10,000 steps at 20,000 K from randomly generated cluster geometries. The five lowest energies from the accepted configurations in the single temperature search were chosen by excluding low energy configurations that were within five MMC steps of a lower energy configuration to improve the diversity of the sampling. Each configuration was used as the starting point of a simulated annealing MMC search that decreased in temperature from 20,000 K to 270 K over 40 temperature changes and a total of 50,000 steps. All MMC calculations were performed within a cube shaped boundary that ensured that the cluster did not dissipate at high temperatures. The dimensions of the cube were chosen so as to not interfere with the simulation beyond stopping dissipation. Geometry optimizations were performed on the lowest energy configurations from the MMC searches at the HF/6-31+G(d,p) level of theory. The fully optimized geometries were confirmed as minima by calculating and diagonalizing the Hessian matrix to test for the presence of imaginary frequencies.

A variation on the nomenclature of Boyd and Boyd[46] is used in this work to characterize the methanol clusters. Cluster configurations in which three or more OH groups form a hydrogen bonded ring structure are labeled X+Y, where X is the number of

methanol molecules involved in the ring structure and Y is the number of methanol molecules that form branching structures adjacent to the hydrogen bonded ring. For example, a cluster with five methanol molecules that are all part of the ring is labeled as 5+0. The same cluster with a single methanol in a branching position and not in the ring is 4+1. Clusters that do not form a ring, but instead form a chain of hydrogen bonded OH groups are labeled "chain". Clusters are classified by visual inspection using MacMolPlt[52] to visualize the cluster configurations.

Octadecane

The minimization of n-octadecane was accomplished by performing a series of single temperature MMC searches with restricted branching. The initial configuration was taken be the fully elongated carbon chain, obtained starting from the optimized structure of hexane. Each carbon atom and the hydrogen atoms directly bonded to that carbon were grouped together, with pair binding constraints added between each set of adjacent carbon atoms with the default max separation value of 1.62 Å. Starting with the fully elongated all-trans configuration, an initial MMC search was completed at 10,000 K. The two lowest and highest accepted energy configurations from the initial MMC search were used as the starting configurations for three MMC searches at 8,000 K, no two configurations coming from adjacent steps in the same search. The highest accepted energy configuration from the initial MMC search is used in the second generation of MMC searches to ensure that the subsequent MMC searches are not limited to sampling configurations near the all-trans initial configuration. The five lowest energy configurations of all three second generation MMC searches were used as the starting

configurations for five MMC searches at 6000 K. Each MMC search included 20,000 steps and the energy was calculated at the MP2/6-31G level of theory[53-57].

Results

Methanol Clusters

The relative energies and cluster conformations of the five lowest energy configurations located with each method via QM/MMC and subsequent geometry optimizations are presented in Table 1. For comparison, the local minima reported by Boyd and Boyd[46] at the B3LYP/6-311+G(d,p)//B3LYP/6-31G(d) level of theory, corresponding to the 5+0, 4+1, and 3+2 conformers, are included in Table 1. The five EFP MMC searches located the 4+1 conformer and four 5+0 conformers shown in Figure 3. Following the MMC searches, the EFP geometries were fully optimized, yielding four unique configurations. The lowest energy FAB QM/MMC configurations (Figure 4) include three 5+0, one 4+1, and one 3+2 conformers in order of increasing energy, in agreement with the previously published DFT conformers. The three 5+0 FAB conformers all optimize to the global minimum, while the 3+2 conformer optimizes to a chain conformation. The FMO QM/MMC simulations failed to locate any configurations with identifiable ring structures, instead forming the elongated hydrogen bonding structures or non-hydrogen bonded diffuse clusters. Four of the five FMO QM/MMC conformers optimize to the same 5+0 conformer that corresponds to the global minimum of the methanol pentamer. The remaining conformer optimizes to a chain conformer. The failure of the FMO QM/MMC method to locate configurations that are close to the fully optimized DFT geometries may be a product of the random nature of the Monte

Carlo method; a more extensive FMO QM/MMC search is likely to produce configurations closer to the predicted minima.

Octadecane

The energies and end-to-end distances of the lowest energy configurations located using a QM/MMC search on n-octadecane with no constraints except for the pair binding constraint on the maximum separation between carbon atoms are presented in Table 2. As one would expect, there is a large decrease in the energy as the temperature decreases. Also, the end-to-end length decreases from 10,000K to 8,000K, and then increases at 6,000K to 19.4 Å compared to the previously reported minimum end-to-end distance of 17 Å. The geometries in Figures 6 show the extent of folding of the n-octadecane chain at the three temperatures. The initial MMC search at 10,000 K distorts the alkane chain away from the elongated starting configuration. The second set of MMC searches at 8,000 K further folds the chain toward the tightly folded state. The lowest energy configurations from the 6,000 K search show a decrease in bond angles and a smoother arc in carbon chain than at the previous temperatures. Based on the large energy difference between the initial configuration and the lowest energy configuration that was located using QM/MMC, the all-trans initial geometry used in this work may not be the best choice. Since the QM/MMC search produced a configuration that is close to the partially folded global minimum of octadecane, and then returned to a less folded structure, it is likely that the starting temperature was not high enough, or the high temperature simulations were not long enough, to get to the global minimum structure. Still, the efficacy of the QM/MMC method for exploring the potential energy surface of

large, internally fragmented molecules with the minimal a priori constraint on the system has been demonstrated.

Conclusion

A QM/MMC method has been implemented for fully ab initio and fragment molecular orbital calculations, as well as the effective fragment potential method. In addition, the pair binding constraint has been introduced as a means of conserving chemical bonds during the MMC search by constraining only the maximum distance between pairs of bonded atoms. The secondary-Monte Carlo method was presented as a means of introducing internal molecular flexibility during the MMC search by performing a Monte Carlo search on the atoms within a unit, when the unit is moved as part of the primary MMC search. To demonstrate the QM/MMC method, the results of MMC searches were performed on the methanol pentamer using the EFP, FMO, and FAB methods, with predicted structures that are consistent with those reported previously.

The folding of n-octadecane from the elongated, all-trans conformer to the partially folded global minimum was used as a test case for pair binding an internally fragmented molecule. Although the extent of the QM/MMC simulations was not sufficient to find the folded global minimum, the method did successfully move away from a fully elongated state to a randomly distributed state and then toward the partially folded state of the global minimum without loss of chemical bonds or external biasing. The QM/MMC method provides variety of tools for investigating chemical systems for which QM accuracy is necessary but the computational cost would otherwise be too expensive.

Acknowledgements

This material is based upon work supported by the Air Force Office of Scientific Research under AFOSR Award No. FA9550-14-1-0306. This work was supported in part by a grant of computer time from the DoD High Performance Computing Modernization Program at the Air Force Research Laboratory DoD Supercomputing Resource Center. Some of the computations reported here were performed on the Iowa State University Cyence cluster, obtained via a National Science Foundation MRI grant, at Iowa State University.

References

1) Metropolis, N.; Ulam, S. J. Am. Stat. Assoc. 44, 335-341 (1949)

2) Metropolis, N. Los Alamos Science 15, 125-130 (1987)

3) Metropolis, N.; Rosenbluth, A. W.; Rosenbluth, M. N.; Teller, A. H.; Teller, E. J. Chem. Phys. 21, 1089-1092 (1953)

4) Hastings, W. K. Biometrika 57, 97-109 (1970)

5) Dubbeldam, D.; Torres-Knoop, A.; Walton, K. S. Mol. Simulat. 39, 1253-1292 (2013)

6) Cornell, W. D.; Cieplak, P.; Bayly, C. I.; Could, I. R.; Merz, K. M. Jr.; Ferguson, D. M.; Spellmeyer, D. C.; Fox, T.; Caldwell, J. W.; Kollman, P. A. J. Am. Chem. Soc. 117, 5179-5197 (1992)

7) Pearlman, D. A.; Case, D. A.; Caldwell, J. C.; Seibel, G. L.; Singh, U. C.; Weiner, P.; Kollman, P. A. AMBER 4.0. San Francisco, CA: University of California Press; 1991.

8) Weiner, P. K.; Kollman, P. A. J. Comp. Chem. 2, 287-303 (1981)

9) Weiner, S. J.; Kollman, P. A.; Case, D. A.; Singh, U. C.; Ghio, C.; Alagona, G.; Profeta S. Jr.; Weiner, P. K. J. Am. Chem. Soc. 106, 765-784 (1984)

10) Weiner, S. J.; Kollman, P. A.; Nguyen, D. T.; Case, D. A. J. Comp. Chem. 7, 230-252 (1986)

11) Jorgensen, W. L.; Madura, J. D.; Swenson, C. J. J. Am. Chem. Soc. 106, 6638-6646 (1984)

12) Jorgensen, W. L.; Swenson, C. J. J. Am. Chem. Soc. 107, 569-578 (1985)

13) Jorgensen, W. L. J. Phys. Chem. 90, 6379-6388 (1986)

14) Jorgensen, W. L. J. Phys. Chem. 90, 1276-1284 (1986)

15) MacKerell, A. D.; Bashford, D.; Bellott, M.; Dunbrack, R. L.; Evanseck, J. D.; Field, M. J.; Fischer, S.; Gao, J.; Guo, H.; Ha, S.; Joseph-McCarthy, D.; Kuchnir, L.; Kuczera, K.; Lau, F. T. K.; Mattos, C.; Michnick, S.; Ngo, T.; Nguyen, D. T.; Prodhom, B.; Reiher, W. E.; Roux, B.; Schlenkrich, M.; Smith, J. C.; Stote, R.; Straub, J.; Watanabe, M.; Wiorkiewicz-Kuczera, J.; Yin, D.; Karplus, M. J. Phys. Chem. B 102, 3586-3617 (1998)

16) Momany, F. A.; Rome, R. J. Comp. Chem. 13, 888-900 (1992)

17) Pavelites, J. J.; Gao, J.; Bash, P. A.; Mackerall, A. D. Jr. J. Comp. Chem. 18, 221-239 (1997)

18) Ponder, J. W.; Wu, C.; Ren, P.; Pande, V. S.; Chodera, J. D.; Schneiders, M. J.; Hague, I.; Mobley, D. L.; Lambrecht, D. S.; DiStasio, R. A. Jr.; Head-Gordon, M.; Clark, G. N. I.; Johnson, M. E.; Head-Gordon, T. J. Phys. Chem. B 114, 2549-2564 (2010)

19) Shi, Y.; Xia, Z.; Zhang, J.; Best, R.; Wu, C.; Ponder, J. W.; Ren, P. J. Chem. Theory Comput. 9, 4046-4063 (2013)

20) Ponder, J. W. TINKER software tools for molecular design. http://

dasher.wustl.edu/tinker

21) Jorgensen, W. L.; Tirado-Rives, J. J. Comput. Chem. 26, 1689-1700 (2005)

22) Shah, J. K.; Maginn, E. J. J. Chem. Phys. 135, 134121 (2011)

23) Dubbeldam, D.; Calero, S.; Ellis, D. E.; Snurr, R. Q. Mol. Simulat. 42, 81-101 (2016)

22) Hillier, I. H. J. Mol. Struct.-THEOCHEM 463, 45-52 (1999)

23) Rocha, W. R.; Coutinho, K.; de Almeida, W. B.; Canuto, S. Chem. Phys. Lett. 335, 127-133 (2001)

24) Wales, D. J.; Hodges, M. P. Chem. Phys. Lett. 286, 65-72 (1998)

25) Dunmar, D. A.; Grayson, M.; Pickup, B. T.; Wilson, M. R. Mol. Phys. 90, 179-187 (1997)

26) Muller-Plathe. F. ChemPhysChem. 3, 754-769 (2002)

27) Jensen, J. H.; Day, P. N.; Gordon, M. S.; Basch, H.; Cohen, D.; Garmer, D. R.; Kraus, M.; Stevens, W. J. Modeling the Hydrogen Bond, 569, 139–151 (1994)

28) Hands, M. D.; Slipchenko, L. V. J. Phys. Chem. B 116, 2775-2786 (2012)

29) Adamovic, I.; Gordon, M. S. J. Phys. Chem. A 110, 10267-10273 (2006)

30) Day, P. N.; Jensen, J. H.; Gordon, M. S.; Webb, S. P.; Stevens, W. J.; Krauss, M.; Garmer, D.; Basch, H.; Cohen, D. J. Chem. Phys. 105, 1968-1986 (1996)

31) Gordon, M. S.; Freitag, M. A.; Bandyopadhyay, P.; Jensen, J. H.; Kairys, V.; Stevens, W. J. J. Phys. Chem. A 105, 293-307 (2001)

32) Gordon, M. S.; Slipchenko, L. V.; Li, H.; Jensen, J.H.. Annual Reports in Computational Chemistry, 3, 177-193 (2007).

33) Webb, S. P.; Gordon, M. S. J. Phys. Chem. A 103, 1265-1273 (1999)

34) Miller, Y.; Thomas, J. L.; Kemp, D. D.; Finlayson-Pitts, B. J.; Gordon, M. S.; Tobias, D. J.; Gerber, R. B. J. Phys. Chem. A 113, 12805-12814 (2009)

35) Smith, Q. A.; Gordon, M. S.; Slipchenko, L. J. Phys. Chem. A 115, 11269-11276 (2011)

36) Patz, C.; Gordon, M.S. To be published.

37) Windus, T.L.; Kathmann, S.M.; Crosby, L.D. J. Phys. Conf. Ser. 125, 012017 (2008)

38) Kitaura, K.; Ikeo, E.; Asada, T.; Nakano, T.; Uebayasi, M. Chem. Phys. Lett. 313, 701-706 (1999)

39) Gordon, M. S.; Fedorov, D. G.; Pruitt, S. R.; Slipchenko, L. V. Chem. Rev. 112, 632-672 (2012)

40) Federov, D. G.; Olson, R. M.; Kitaura, K.; Gordon, M. S.; Koseki, S. J. Comp. Chem. 25, 872-880 (2004)

41) Day, P. N.; Pachter, R.; Gordon, M. S.; Merrill, G. N. J. Chem. Phys. 112, 2063-73(2000)

42) Wales, D. J.; Hodges, M. P. Chem. Phys. Lett. 286, 65-72 (1998)

43) Li, Z.; Scheraga, H. A. Proc. Nat. Acad. Sci. USA 84, 6611(1987).

44) Kazachenko, S.; Bulusu, S.; Thakkar, A. J. J. Chem. Phys. 138, 224303 (2013)

45) Hagemeister, F. C.; Gruenlob, C. J.; Zwier, T. S. J. Phys. Chem. A 102, 82-94 (1998)

46) Boyd, S. L.; Boyd, R. J. J. Chem. Theory Comput. 3, 54-61 (2007)

47) Lüttschwager, N. O. B.; Wassermann, T. N.; Mata, R. A.; Suhm, M. A. Angew. Chem. Int. Ed. 52, 463-466 (2013)

48) Sun, L.; Siepmann, J. I.; Schure, M. R. J. Chem. Theory Comput. 3, 350-357(2007)

49) Ferguson, A. L.; Debenedetti, P. G.; Panagiotopoulos, A. Z. J. Phys. Chem. B 113, 6405-6414 (2009)

50) Schmidt, M. W.; Baldridge, K. K.; Boatz, J. A.; Elbert, S. T.; Gordon, M. S.; Jensen, J. J.; Koseki, S.; Matsunaga, N.; Nguyen, K. A.; Su, S.; Windus, T. L.; Dupuis, M.; Montgomery, J. A. Jr. J. Comput. Chem. 14, 1347-1363 (1993)

51) Gordon, M. S.; Schmidt, M. W. Advances in Electronic Structure Theory: GAMESS a Decade Later. In Theory and Applications of Computational Chemistry; Dykstra, C. E.; Frenking, G.; Kim, K. S.; Scuseria, G. E. Eds; Elsevier, Amsterdam, The Netherlands, 2005; chapter 41, pp 1167-1189

52) Bode, B. M.; Gordon, M. S. *J. Mol. Graphics and Modeling*, **16**, 133-138 (1999)

53) Møller, C.; Plesset, M. S. Phys. Rev. 46, 618 (1934).

54) Ditchfield, R.; Hebre, W. J.; Pople, J. A. J. Chem. Phys. 54, 724-728 (1971)

55) Hehre, W. J.; Ditchfield, R.; Pople, J. A. J. Chem. Phys. 56, 2257-2261 (1972)

56) Hariharan, P. C.; Pople, J. A. Theoret. Chem. Acta. 28, 213-222 (1973)

57) Clark, T.; Chandrasekhar, J.; Spitznagel, G. W.; Schlever, P. von R. J. Comput. Chem. 4, 294-301 (1983)

Table 1: Energy and conformer of lowest energy configurations from MMC search

	QM/MMC results		Optimized results	
Method	Energy (kcal/mol)[a]	Conformer	Energy (kcal/mol)[a]	Conformer
EFP-1	3.8703	4+1	0.2522	4+1
EFP-2	5.4589	4+1	0.4216	5+0
EFP-3	5.5753	5+0	0.2980	5+0
EFP-4	5.6829	5+0	0.0000	5+0
EFP-5	6.0886	5+0	0.0000	5+0
FAB-1	11.4193	5+0	0.0000	5+0
FAB-2	13.9101	5+0	0.0003	5+0
FAB-3	15.9744	5+0	0.0055	5+0
FAB-4	20.5060	4+1	4.3701	4+1
FAB-5	24.4401	3+2	6.2475	linear
FMO-1	23.1356	N/A[b]	0.0000	5+0
FMO-2	27.5163	N/A[b]	0.0007	5+0
FMO-3	30.5604	N/A[b]	6.2010	linear
FMO-4	30.6680	N/A[b]	0.0000	5+0
FMO-5	21.3208	N/A[b]	0.0007	5+0
DFT-1[c]			0.0000	5+0
DFT-2[c]			0.2196	5+0
DFT-3[c]			1.1546	5+0
DFT-4[c]			3.3697	4+1
DFT-5[c]			12.2363	3+2

[a]Relative to lowest energy optimized configuration for each method [b]Neither ring or chain structure exist at lowest energy configurations. [c]Ref. 46.

Table 2: Energy and end-to-end distance of lowest energy octadecane configurations.

Temperature (K)	Relative Energy (kcal/mol)	End-to-end distance (Å)
Initial	0	21.06
10,000	-233	20.83
8,000	-347	16.63
6,000	-377	19.36

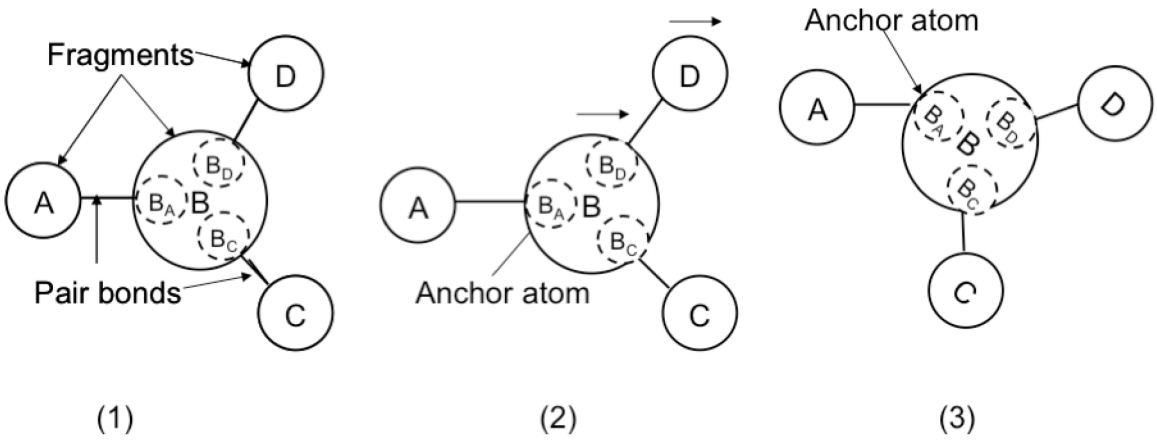

Figure 1. Effect of MMC movements on three or more fragments that are pair bound to each other. (1) Units A, C, and D are pair bound to unit B (solid circles) at the atoms B_A, B_C, and B_D, (dashed circles) respectively. (2) Translation of B with anchor atom B_A is propagated so that B, C, and D undergo the same translation. (3) Rotation of B around anchor atom B_A is propagated such that B, C, and D rigidly rotate around B_A.

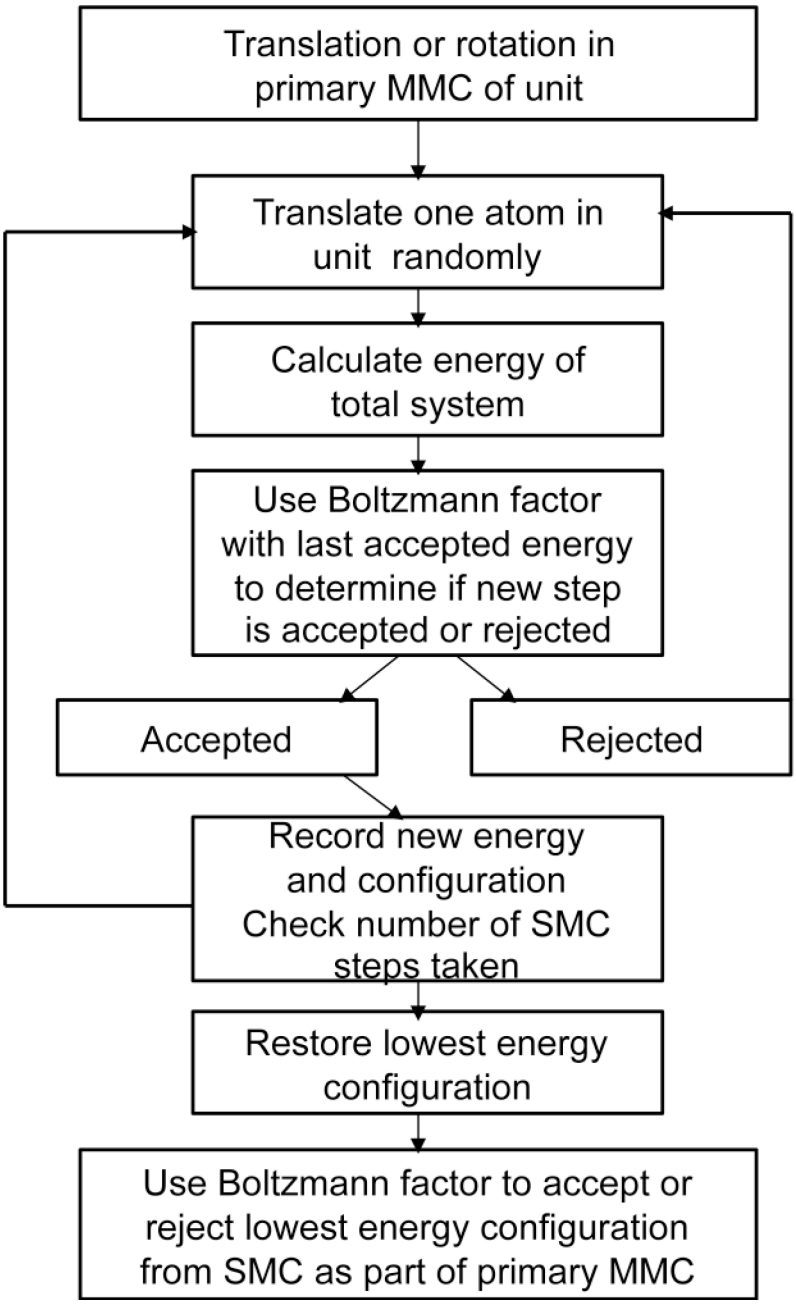

Figure 2. Flowchart of steps taken during the secondary Monte Carlo search.

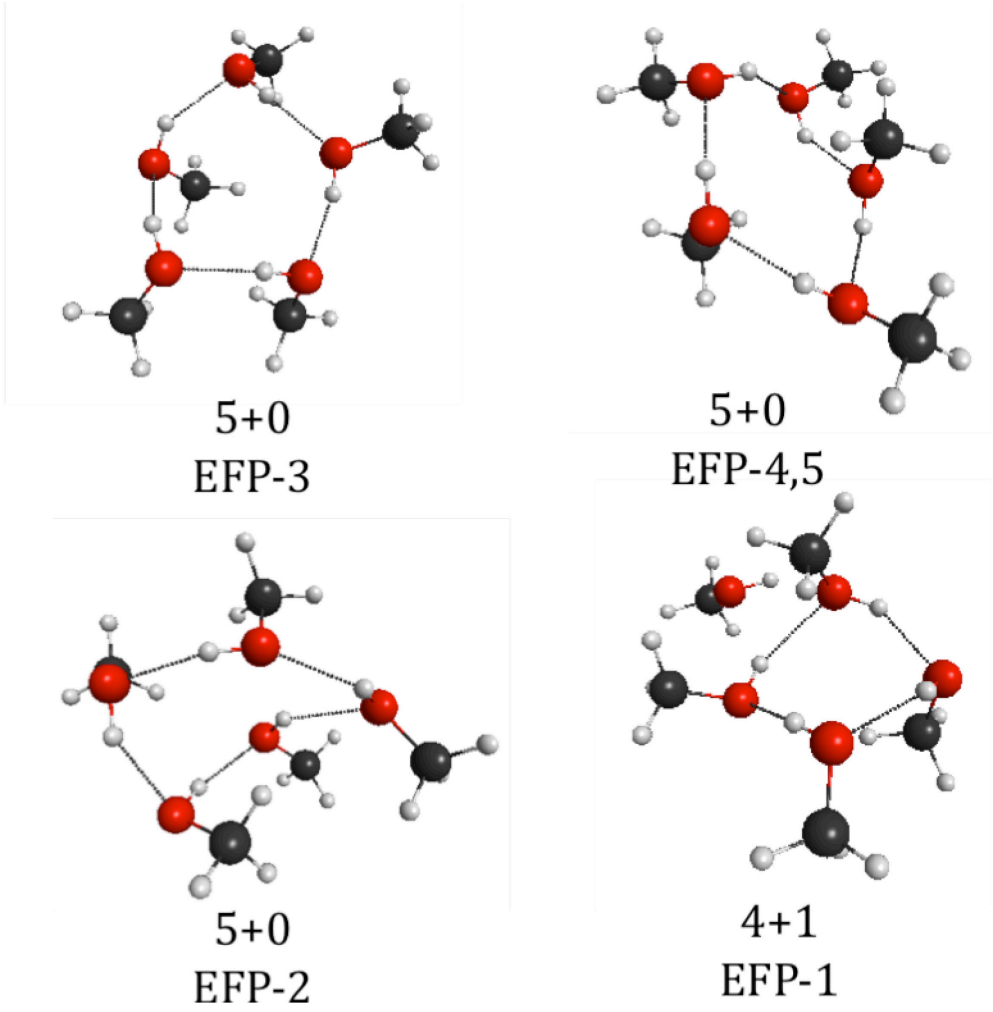

Figure 3. Unique optimized geometries starting from lowest energy configurations located with five EFP QM/MMC searches of methanol pentamer. Dotted lines added to emphasize connection. Pentamer labels correspond to entry numbering in Table 1.

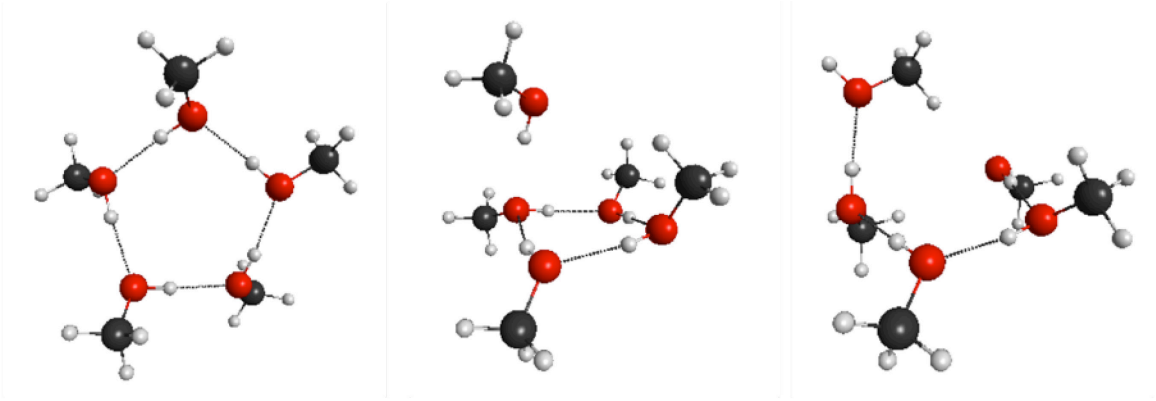

Figure 4. Unique optimized geometries starting from lowest energy configurations located with five FAB QM/MMC searches of methanol pentamer. Dotted lines added to emphasize connection. Pentamer labels correspond to entry numbering in Table 1.

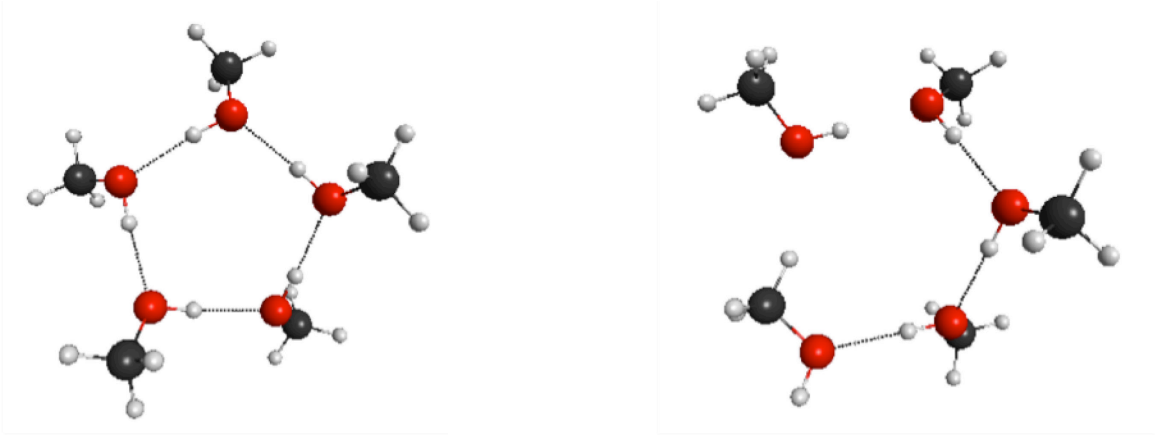

Figure 5. Unique optimized geometries starting from lowest energy configurations located with five FMO QM/MMC searches of methanol pentamer. Dotted lines added to emphasize connection. Pentamer labels correspond to entry numbering in Table 1.

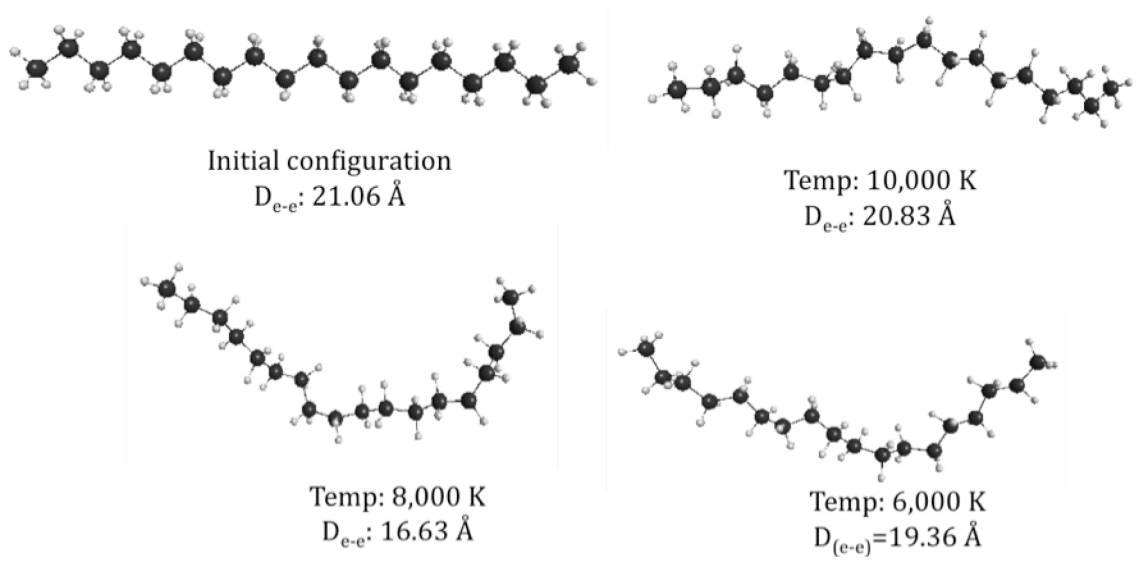

Figure 6. Lowest energy configurations of n-octadecane from MMC searches with listed temperature and end-to-end distance (D_{e-e}) showing partially folded structure. Initial all-trans configuration included for reference.

CHAPTER 5: RATIO-OF-STATES MONTE CARLO METHOD

Caleb Carlin and Mark S. Gordon

Abstract

Accurately calculating the equilibrium constant of a reaction that occurs in bulk liquid using quantum mechanical methods poses a significant challenge and cost. A new method is presented based on the Metropolis Monte Carlo method, called the ratio-of-states method, for the calculation of equilibrium constants in solvated systems. The anionic system of H_2S and NH_3 with an excess electron is tested using the ratio-of-states method to determine the impact of the choice of state sorting criteria, temperature, and starting configuration on the accuracy of the ratio-of-states method. The results suggest that the choice of state sorting criteria and starting configuration significantly impact the accuracy of the calculated equilibrium constant, but the temperature used does not.

Introduction

Protic ionic liquids [PILs] are molten salts with melting temperatures below 100 °C, formed by the proton transfer between a Bronsted acid and base[1]. Unlike traditional salts, PILs exist as mixtures of ions and neutral pairs in the liquid phase[2]. The degree to which the proton transfer equilibrium lies on the side of ions in a PIL, or ionicity, has been shown to play a role in determining properties exhibited by the PILs, such as solubility, enthalpy of vaporization, and surface tension[3]. The primary method for experimentally determining the ionicity of PILs is to plot the effective ion conductivity vs. the inverse of the viscosity at different temperatures or molar concentrations compared to an ideal salt, generally potassium chloride[4,5]. On the resulting graph, called

a Walden plot, ionicity has a negative correlation with the separation between the slope of the PIL and the slope of the ideal salt. Improved Walden methods exist that account for the size of the ions and the conductance produced by the diffusion of ions[6]. However, the experimental methods have only qualitative accuracy and are applicable to only a subset of ionic liquids with a specific trait like NMR active nuclei[6].

The computational approach to calculating ionicity is to determine the equilibrium constant (K_{eq}) of the proton transfer reaction. However, calculating the K_{eq} by directly simulating a bulk liquid is prohibitively expensive, leading researchers to pursue approximations to the K_{eq}. The difference in the aqueous acid dissociation constants of the acid and the base (eqn. 1) has been proposed as one approximation of the K_{eq} with mixed results[2].

$$\Delta pK_a^{aq} = \left| pK_{acid}^{aq} - pK_{base}^{aq} \right| \quad (1)$$

Equilibrium calculations indicate that a ΔpK_a^{aq} of 4 should be sufficient for complete proton transfer or high ionicity in PILs, but experiments show that complete proton transfer occurs only in some PILs that have a ΔpK_a^{aq} of 10 or greater[3]. A study involving super-strong bases found that ionicity increases with increasing ΔpK_a^{aq} up to a maximum at ΔpK_a^{aq}=15, and then remains constant[5]. However, a study of primary and tertiary amines found that the correlation between ΔpK_a^{aq} and ionicity depends on the structure of the cation and the proton-binding site[7]. A cation bound to a primary amine demonstrates high ionicity with ΔpK_a^{aq}=2 like a traditional salt, while a cation bound to a tertiary amine demonstrates low ionicity despite having a ΔpK_a^{aq}=6. The failure of ΔpK_a^{aq} to

predict ionicity is attributed to the effect of intermolecular interactions of PILs, which are poorly approximated in an aqueous environment.

An improved method for approximating the K_{eq} must simulate the PIL environment at a computational cost that is not prohibitive. A study by Izgorodina, Forsyth, and MacFarlane demonstrated that quantum mechanical (QM) methods are necessary for accurately simulating PILs by demonstrating the impact of dispersion forces on the behavior of imidazolium based PILs[8]. QM methods that include the dispersion energy are abundant, but come at a steep cost compared to classical methods. Møller-Plesset second order perturbation theory (MP2)[9] scales formally as N^5 for both energy and gradient calculations, where N represents the size of the basis set, while classical methods scale as N^2. Although the exact number of cations and anions necessary to represent a PIL environment is unknown, mass spectrometry measurements of aerosolized ionic liquid clusters have determined that clusters with fewer than 12 ion pairs are unstable and quickly vaporize[10]. Simulating an ionic liquid cluster with 12 ion pairs using a method that depends on the gradient of the wavefunction like molecular dynamics is presently untenable on all but the largest computers.

The Metropolis Monte Carlo (MMC) method requires only the calculation of the total energy of the system[11], and can be adapted to predict a wide range of non-dynamic chemical properties. The Widom insertion method[12], for example, can be used to calculate the chemical potential of a molecule within a solvent environment by solving for the energy difference between E_s and E_{s+X} , the total energy of the solvent system (s) and the total energy of the solvent plus test molecule system (s+X) respectively[13]. An MMC search is used to generate an ensemble of solvent configurations and the test

molecule is inserted at random positions within the configurations, and the change in energy is calculated. Averaging over all insertions in the ensemble allows one to calculate properties of the test molecule in the system, such as the chemical potential and concentration. However, locating a position to insert the test molecule without overlapping solvent molecules quickly becomes nearly impossible as the test molecule size increases, leading to oversampling of high-energy configurations. In general, PILs are too large for the Widom insertion method to be a viable option.

In this work the Ratio-of-States (ROS) Monte Carlo method for predicting the K_{eq} of proton transfer reactions is presented. Consider the transfer of a proton (H^+) between an acid (A) and a base (B) as in reaction 2.

$$HA + B \rightarrow A^- + HB^+ \tag{2}$$

The K_{eq} for reaction 2 is given as the ratio of the concentrations of the products and reactants at the equilibrium state.

$$K_{eq} = \frac{[A^-][HB^+]}{[HA][B]} \tag{3}$$

Simulating a bulk chemical system that is large enough for the concentrations of the reactants and products is not feasible without access to super computers. Sampling a smaller but representative system in the time or phase space can approximate the concentration of reactants and products, if the method used for sampling is ergodic. Ergodicity describes the ability of a method to completely sample a chemical system independent of the starting state in the limit of an infinite number of sample steps[14]. MMC methods are assumed to be ergodic and can be used to approximate the

concentrations of reactants and products in an equilibrium chemical system. A representative system containing one of each of three species, A, B, and H^+, in a QM core surrounded by a cluster of solvent molecules may be defined as being in a reactant state, a product state, or neither, depending solely on the positions of the core atoms according to some specified criteria. An ensemble of states of the chemical system is generated by MMC sampling of the core and cluster coordinates and their associated energies. If the ensemble is generated using J MMC searches, then the concentration of the acid, as measured by counting the number of reactant states, is given by Equation 4.

$$[HA] = \frac{\sum_{x}^{J} N_x R_x}{\sum_{x}^{J} N_x} \tag{4}$$

Here the sum is over the results of the J MMC searches while N_x and R_x are the number of accepted steps and the number of states, respectively, that are determined to be reactant states in each MMC search. A similar equation defines the concentrations of the product species, substituting P_x for R_x as the number of accepted states that are determined to be products. Note that the presence of one species (e.g., reactant HA) implies the presence of it complement (e.g, reactant B). Therefore, one can substitute the appropriate concentrations into Equation 3 as follows.

$$K_{eq} = \frac{\left(\sum_{x}^{J} (N_x P_x)\right)^2}{\left(\sum_{x}^{J} (N_x R_x)\right)^2} \tag{5}$$

Here again, the sum is over the results of all J MMC searches used to generate the ensemble. In the case of a single MMC search, Equation 5 reduces to the square of the simple ratio of the number of product states to reactant states in the phase space of the chemical system. The larger the ensemble of sampled states, the more accurate the approximation. However, since the number of degrees of freedom of the solvent cluster is significantly larger than the number of degrees of freedom of the core, much of the phase space does not contribute significantly to the ratio of states. It is therefore preferable to constrain the sampling to perturbations of the core. The recently developed pair binding Metropolis Monte Carlo method (See chapter 4) facilitates such a constrained search.

The details of the pair binding in the QM/MMC method are presented elsewhere[15], so only a brief summary is presented here. Two groups of atoms are pair bound by specifying an atom in each group, called anchor atoms, and a maximum separation between the two atoms. Any movement of either group during the course of the MMC search is rejected if the distance between the two atoms exceeds the maximum separation. If a group is pair bound to more than one group, then all such movements are propagated through the network of connected groups. For the ROS method, A and B are each pair bound to the H^+ through anchor atoms designated as the acid anchor (AA), and base anchor (BA), respectively (Figure 1). The maximum allowed separation between the acid and the proton, and between the base and the proton are labeled D_{AH} and D_{BH}, respectively. Whether a configuration is in the reactant or product state is defined by the quantities R_{AH} and R_{BH}, such that if the separation between AA and H^+ is less than R_{AH}, then the configuration is a reactant state. Likewise, if the separation between BA and H^+

is less than R_{BH}, then the configuration is a product state. If both separations between anchor atoms and the proton are less than the respective cutoff separations, then the pair binding with the smallest absolute separation is used for the purpose of determining the state. The possibility that the separations between AA, BA, and H^+ are smaller than both R_{AH} and R_{BH} arises because cutoff distances can be longer than the AA-H^+ and BA-H^+ bond lengths. If neither separation is less than the cutoffs, then the configuration is neither a reactant nor a product state.

Performing a constrained MMC search significantly reduces the number of steps needed to adequately sample the phase space of interest. Further savings may be accomplished by employing the Effective Fragment Potential (EFP)[16-19] method to calculate the interactions between the solvent and the core. The EFP model, a semi classical method with parameters derived entirely from QM calculations, has been shown to successfully reproduce the solvation of ions and water-alcohol mixtures[20-24].

To demonstrate the ROS method, the proton transfer reaction between hydrogen sulfide and ammonia with an excess electron attached in a water environment is evaluated. Hydrogen sulfide and ammonia are byproducts of the gasification of biomass processes and precursors of toxic emissions including NO_x and sulfur dioxide[25,26]. A computational study of the proton transfer from hydrogen sulfide to ammonia at the B3LYP/6-31++G(5d) level of theory determined that the reaction has no clear transition state[27]. Introducing an additional electron into the reaction system changes the potential energy surface to a pair of potential energy wells separated by a clear energy barrier along the reaction coordinate. The activation energy for the hydrogen sulfide and ammonia system with an extra electron was determined to be 1.76 kcal/mol with an

activation energy for the reverse process of 0.94 kcal/mol[27]. Using the reported first acid dissociation constants for hydrogen sulfide and ammonium ($8.9*10^{-8}$, $5.6*10^{-10}$)[28], the K_{eq} for the neutral system is $6.52*10^{-3}$. The impact of the excess electron on the K_{eq} has not been previously evaluated. However, the addition of an excess electron has been shown to induce a proton transfer between HCl and NH_3 that does not occur without the excess electron[29]. In addition, the presence of the excess electron in the H_2S-NH_3 system introduces a minimum in the potential energy surface of the proton transfer corresponding to the products[28]. Therefore, it is reasonably assumed that the addition of the excess electron shifts the equilibrium state toward the products and the neutral equilibrium constant is only a lower bound on the equilibrium constant of the anionic system.

The ROS Method

The initial step in the ROS method is to determine the key parameters of the ROS/MMC searches, including the temperature, the sorting criteria, the pair binding maximum separation, and the number of solvent molecules to include in the cluster. Locating the gas phase transition state of the proton transfer reaction is generally an effective means of identifying the best parameters for the system of interest. However, trial and error is a viable, if more expensive, approach to optimizing the parameters.

Once the system dependent parameters have been determined, the ROS method proceeds in two stages: generating the cluster and perturbing the core. The starting configuration is generated by randomly placing the solvent molecules into a cluster around the core, which is held immobile. Then the cluster is frozen in place while a

MMC search is carried out on the groups in the core. Any step that is accepted as part of the MMC search is tested against the state sorting criteria, and a count is maintained of the number of reactant and product states located. The process is repeated to generate the ensemble, each time starting with a new, randomly generated cluster configuration. When the MMC searches are completed, the K_{eq} is calculated using Equation 5.

Influencing Factors

The ROS method approaches the exact K_{eq} in the limit of an infinite, unconstrained MMC search. However, it is unknown to what extent variations in the parameters affect the accuracy of the ROS/MMC search. In this work, those factors are explored using a simple test case to determine the extent of the impact that each factor has on the accuracy of the calculated K_{eq}. The factors studied in the present work are the temperature, the state sorting criteria, and the starting position of the proton relative to the acid and base.

The temperature determines the likelihood that a step in the MMC search that increases the total energy will be accepted. If the temperature is too low relative to the activation energy, the MMC search may become trapped on one side of the transition state, failing to sample the entire reaction path. If the temperature is too high, then the MMC will accept every step without regard to the change in energy. To test the impact of temperature on the ROS method, five temperatures were chosen based on the activation energy for the proton transfer in the test case. The initial temperature was chosen to be 740 K; at this temperature a step from the reactant minimum to the transition state will be accepted with a 30% probability. The remaining temperatures (1183 K, 961

K, 518 K, and 296 K) were chosen to be greater than or less than 740 K by 22% or 60% to test the impact of both small and large changes in the temperature in a symmetric approach.

An ergodic system that is perturbed using the MMC method with an infinite number of steps will sample the entire phase space independent of the starting configuration. In practice, the starting position of the proton in the core should not affect the final ratio of states unless the search is trapped on one side of the energy barrier or if the sampling is too small. However, as the ROS method benefits from performing many short MMC searches with different cluster configurations, it is not guaranteed that the final results will be independent of the starting position. To test the impact of the starting position of the proton, three starting configurations for the core are tested corresponding to the transition state (T_s) and 0.1 Å perturbations toward the reactant (T_{s-1}) and product (T_{s+1}) states.

Accurate criteria for separating whether sampled states are reactants or products are vitally important for the ROS method. Three possible approaches for setting the criteria are tested in the present work; reactant/product geometries (GM), the transition state (TS), and the van der Waals radii (VDW). The cutoff distances (R_{AH}, R_{BH}) for each approach given in Table 1 were chosen based on the end state minima and transition state reported by Dong and Wang[27] and the accepted van der Waal radii of sulfur, nitrogen, and hydrogen. If one bases the criteria on the equilibrium bond lengths at the optimized geometry end points of the proton transfer reaction, there is a narrow range of configurations that most closely represent pure reactant states or pure product states. However, the short cut off distances can result in too few data points to derive

meaningful results. Defining the state sorting criterion using the AA-H^+ and BA-H^+ bond lengths at the transition state separates the reaction pathway such that any deviation from the transition state is labeled a reactant or product state. The transition state approach is more inclusive than the end point geometries approach, and the potential energy surface of the system still influences the configuration assignments. Defining the criteria based on the van der Waals radii of the H^+, AA, and BA is both the most expansive and generic of the approaches.

Computational Methods

All calculations were completed using GAMESS[30,31] at the MP2/cc-pVTZ[32] level of theory with ROHF for the doublet calculations. To test the impact of the identified factors, 45 ROS/MMC searches of 10,000 steps each were completed, representing all possible combinations of the three test parameters. All ROS/MMC searches were performed with a cluster of 64 water molecules modeled using EFP with the EFP1 parameters programmed into GAMESS.

Results and Discussion

Sorting criteria

The equilibrium constant K_{eq} for the proton transfer reaction has been calculated using Equation 5 with all temperatures and starting positions for each state sorting criteria. The GM and TS criteria reproduce the experimental neutral K_{eq} to within half an order of magnitude, as shown in Table 2. The VDW criterion yields a calculated K_{eq} that is larger than the experimental K_{eq} by a factor greater than 10. Without knowing how the excess electron changes the K_{eq} of the neutral system, it is impossible to say how

accurately the VDW criterion reproduces the K_{eq}. The GM and TS criteria fail to produce K_{eq}'s that are greater than the lower bound set by the experimental K_{eq}. The proposed explanation for the failure of the GM and TS criteria is that the narrow state criteria in tandem with the number of steps in the MMC searches introduces error due to under-sampling. Therefore, it is recommended that the GM and TS criteria only be used with extended MMC searches. The success of the VDW criterion is indicative of how the reaction pathway of the proton transfer is a poor representation of the phase space sampled by the ROS/MMC. The pair binding constraint allows configurations that are not part of the reaction pathway, but still contribute to the K_{eq}. The large separation cutoffs of the VDW criterion result in the most complete ensemble of the three criteria tested.

Temperature

The temperature of the ROS/MMC search determines the probability that a step in the MMC search will cross the transition state from the reactant to product state or the reverse. Multiple ROS/MMC searches at the same temperature that fail to sample both the reactant and product states suggests that temperature is too low for the reaction under investigation to cross the barrier. The percentage of ROS/MMC searches that sampled only a single state, separated by temperature and state sorting criteria, is presented in Table 3. For all three criteria, the change in percentage of single state searches is independent of the change in temperature within the error of the calculation, with the exception of the 961 K and 1183 K percentages for the TS and GM criteria. However, no trend exists for these criteria, a large percentage of single state searches for one temperature is matched with a small percentage for the other temperature. The range in

values for each criteria negatively correlates with the length of the separation cut offs of each criteria. The observed correlation is due to the decreased number of data points as the separation cutoffs decrease. Accounting for the variance of the TS and GM criteria, the small trend of increasing percentage with increasing temperature is not statistically significant for the number of MMC searches included in this work. It is concluded that the ROS method is minimally affected by changes in temperature.

Starting configuration

To assess the impact of the starting configuration of the core on the probability that the ROS/MMC search will sample both the reactant and product state, the percentage of searches performed that only sampled the reactant state was calculated for each starting position and for each of the three criteria. To clarify the impact of starting position on the likelihood of the search being trapped in one state, the two searches that sampled the product state only are excluded from this discussion. The results for the TS criterion in Table 4 show a high instance (68%) of the MMC search being trapped in the reactant state starting from the T_{s-1} position. The instances of single state sampling starting from the T_s and T_{s+1} positions are likely due to the topography of the potential energy surface of the reaction, and not representative of biased sampling caused by the initial configuration. For the GM criterion, the difference in the percentage of single state searches between T_{s-1} and T_{s+1} is 16%; this amounts to 5 more single state searches from the T_{s+1} position than the T_{s-1} position. The results for the VDW criterion similarly show an increased likelihood of sampling only the reactant state starting from the T_{s-1} and T_s positions. While a clear impact on the outcome of the ROS/MMC search cannot be

established, it is concluded that the transition state is the optimum starting configuration if it is known.

Limitations and future work

The present work introduces the ROS method and analyzes three factors that can influence the accuracy of the method. However, the limited number of ROS/MMC searches limits meaningful interpretation of the results. Chemically meaningful results with the ROS method are attained when the calculated equilibrium converges and does not change further with an increase in the number of MMC steps. A full test of the ROS method requires the calculation of the K_{eq} using a single set of parameters and an increasing number of MMC searches until the computed equilibrium constant converges. In addition, the choice of a basis set without diffuse is likely a poor choice for a charged system such as tested here. Future work will provide more extensive testing and evaluation, including the use of a more appropriate basis set.

Conclusion

In this work, the ROS method was introduced as a tool for calculating the K_{eq} of a proton transfer reaction in an aqueous or non-aqueous environment. Using pair binding to constrain a MMC search to the phase space of the proton transfer reaction, each accepted step in the MMC search is labeled a product state, a reactant state, or neither. The weighted average of the number of product and reactant states identified over all MMC searches is used to calculate the squared ratio of the number of product and reactant states. The squared ratio is equal to the K_{eq} of the proton transfer reaction as the number of states sampled increases to the limit of an infinite number of steps. To test the

impact of the choice of three parameters, the proton transfer between H_2S and NH_3 with an excess electron has been studied using the ROS method. The choice of state sorting criterion was shown to have the largest impact on the accuracy followed by the choice of the starting configuration of the core molecules. The choice of temperature was shown to not impact the sampling of states over a range of 867 degrees K. Upon further successful testing, the ROS method can be applied to calculating the K_{eq}s of systems like ionic liquids that are otherwise prohibitively difficult to determine.

Acknowledgements

This material is based upon work supported by the Air Force Office of Scientific Research under AFOSR Award No. FA9550-14-1-0306. This work was supported in part by a grant of computer time from the DoD High Performance Computing Modernization Program at the Air Force Research Laboratory DoD Supercomputing Resource Center.

References

1) Greaves, T. L.; Drummond, C. J. Chem. Rev. 108, 206-237 (2008)

2) Johansson, K. M.; Izgorodina, E. I.; Forsyth, M.; MacFarlane, D.R.; Seddon, K. R. Phys. Chem. Chem. Phys. 10, 2972-2978 (2008)

3) Yoshizawa, M.; Xu, W.; Angell, C. A. J. AM. CHEM. SOC. 125, 15411-15419 (2003)

4) Ueno, K.; Tokuda, H.; Watanabe, M. Phys. Chem. Chem. Phys. 12, 1649-1658 (2010)

5) Miran, M. S.; Kinoshita, H.; Yasuda, T.; Susan, Md. A. B. H.; Watanabe, M. Phys. Chem. Chem. Phys. 14, 5178-5186 (2012)

6) Schreiner, C.; Zugmann, S.; Harti, R.; Gorea, H. J. J. Chem. Eng. Data 55, 1784-1788 (2010)

7) Stoimenovski, J.; Izgorodina, E. I.; MacFarlane, D. R. Phys. Chem. Chem. Phys. 12, 10341-10347 (2010)

8) Izgorodina, E. I.; Forsyth, M.; MacFarlane, D. R. Aust. J. Chem. 60, 15-20 (2007)

9) Moller, C.; Plesset, M. S. Phys. Rev. 46, 618-621 (1934)

10) Hogan, C. J. Jr.; Mora, J. F. de la; J. Am. Soc. Mass Spectrom. 21, 1382-1286 (2010)

11) Metropolis, N.; Ulam, S. J. Am. Statis. Assoc. 44, 335-341 (1949)

12) Widom, B. J. Chem. Phys. 39, 2808 (1963)

13) Sulpizi, M.; Sprik, M. J. Phys. Condens. Matter 22, 283116-284124 (2010)

14) Li. Z.; Scheraga, H. A. Proc. Natl. Acad. Sci. 84, 6611-6615 (1987)

15) Carlin, C.; Gordon, M. S. to be published

16) Jensen, J. H.; Day, P. N.; Gordon, M. S.; Basch, H.; Cohen, D.; Garmer, D. R.; Kraus, M.; Stevens, W. J. Modeling the Hydrogen Bond, 569, 139–151 (1994)

17) Day, P. N.; Jensen, J. H.; Gordon, M. S.; Webb, S. P.; Stevens, W. J.; Krauss, M.; Garmer, D.; Basch, H.; Cohen, D. J. Chem. Phys. 105, 1968-1986 (1996)

18) Gordon, M. S.; Freitag, M. A.; Bandyopadhyay, P.; Jensen, J. H.; Kairys, V.; Stevens, W. J. J. Phys. Chem. A 105, 293-307 (2001)

19) Gordon, M. S.; Slipchenko, L. V.; Li, H.; Jensen, J.H.. Annual Reports in Computational Chemistry, 3, 177-193 (2007).

20) Hands, M. D.; Slipchenko, L. V. J. Phys. Chem. B 116, 2775-2786 (2012)

21) Adamovic, I.; Gordon, M. S. J. Phys. Chem. A 110, 10267-10273 (2006)

22) Webb, S. P.; Gordon, M. S. J. Phys. Chem. A 103, 1265-1273 (1999)

23) Miller, Y.; Thomas, J. L.; Kemp, D. D.; Finlayson-Pitts, B. J.; Gordon, M. S.; Tobias, D. J.; Gerber, R. B. J. Phys. Chem. A 113, 12805-12814 (2009)

24) Patz, C.; Gordon, M.S. To be published

25) Torres, W.; Pansare, S. S.; Goodwin, J. G. Jr. Catalysis Reviews 49, 407-456 (2007)

26) Laudenslager, J. B.; Huntress, W. T. Jr. Int. J. Mass Spectrom. 14, 435-448 (1974)

27) Dong, L.; Wang, J. Computational and Theoretical Chemistry 983, 85-100 (2012)

28) W. M. Haynes, ed., CRC Handbook of Chemistry and Physics, 96th Edition (Internet Version 2016), CRC Press/Taylor and Francis, Boca Raton, FL.

29) Eustis, S. N.; Radisic, D.; Bowen, K. H.; Bachorz, R. A.; Haranczyk. M. Science 319, 936-939 (2008)

30) Schmidt, M. W.; Baldridge, K. K.; Boatz, J. A.; Elbert, S. T.; Gordon, M. S.; Jensen, J. J.; Koseki, S.; Matsunaga, N.; Nguyen, K. A.; Su, S.; Windus, T. L.; Dupuis, M.; Montgomery, J. A. Jr. General Atomic and Molecular Electronic Structure System. J. Comput. Chem. 1993, 14, 1347-1363.

31) Gordon, M. S.; Schmidt, M. W. Advances in Electronic Structure Theory: GAMESS a Decade Later. In Theory and Applications of Computational Chemistry; Dykstra, C. E.; Frenking, G.; Kim, K. S.; Scuseria, G. E. Eds; Elsevier, Amsterdam, The Netherlands, 2005; chapter 41, pp 1167-1189

Table 1. Separation cutoffs used for state sorting criteria

State Criteria	R_{AH} (Å)	R_{BH} (Å)
TS	1.64	1.35
GM	1.40	1.13
VDW	3.00	2.75

Table 2: Equilibrium constants calculated using three state sorting criteria

State Criteria	K_{eq}
TS	5.92E-03
GM	6.13E-03
VDW	8.46E-02
Experiment	6.52E-03

Table 4: Percentages of ROS/MMC searches that sampled only the reactant state based on starting position and state sorting criteria

Starting Position	State Criteria		
	TS	GM	VDW
T_{S-1}	68%	64%	4%
T_S	24%	76%	8%
T_{S+1}	8%	80%	0%

Table 4: Percentages of ROS/MMC searches that sampled only the reactant state based on starting position and state sorting criteria

Starting Position	State Criteria		
	TS	GM	VDW
T_{S-1}	68%	64%	4%
T_S	24%	76%	8%
T_{S+1}	8%	80%	0%

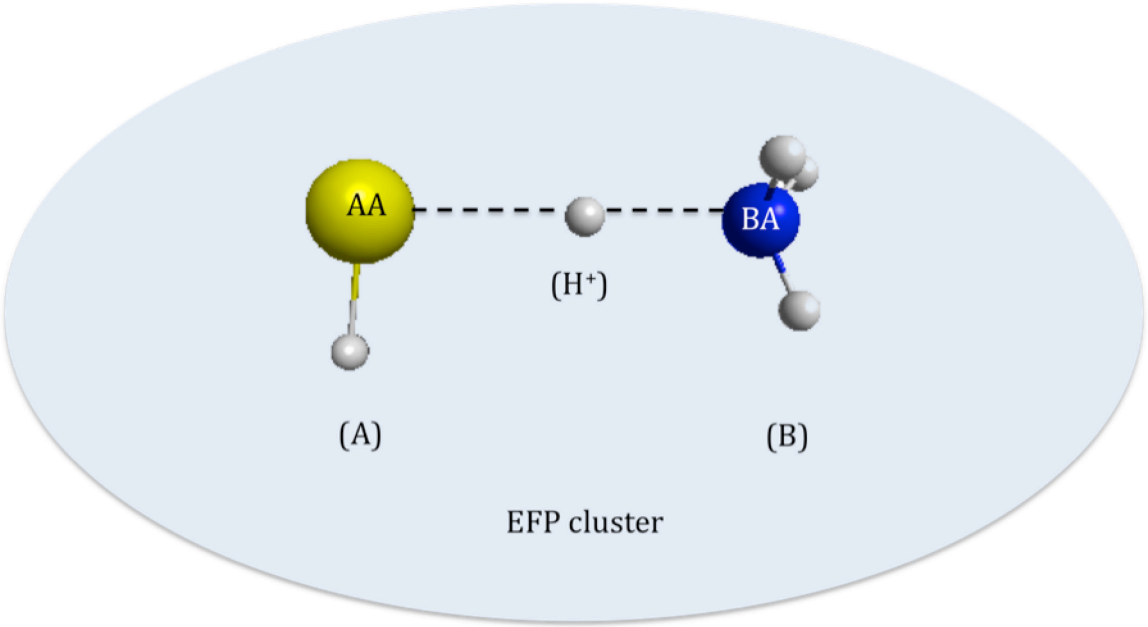

Figure 1. Division of $[H_2S\text{-}NH_3]^-$ system for ROS method. The ab initio core is divided into three groups (A, B, H^+) and connected by pair binding (dotted lines) between the acid anchor (AA) and base anchor (BA) through the proton (H^+). The ab initio core is surrounded by a randomly positioned cluster of EFP waters.

CHAPTER 6: CONCLUSION

In chapter 2, two methods were used to calculate the PAs and IPs for a set of anions to determine the accuracy and efficiency of both methods. It has been demonstrated that both MP2 and CR-CC(2,3) produce PAs with similar accuracy compared to experiment. Therefore, the less computationally demanding MP2 method appears to be reliable for the prediction of ionic liquid PAs. For IPs, the CR-CC(2,3) method produces significantly more accurate values compared to experiment than does MP2. For most species studied, the CR-CC(2,3) method predicts IPs that are in good agreement with the experimental values. However, for molecules that have degenerate frontier orbitals, such as ClO_4^-, it is important to use a multi-configuration reference wave function, in order to accommodate fractional orbital occupancy.

In chapter 3, the calculated deprotonation energies of selected ionic liquid cations of interest are presented as well as the net energies for the proton transfer reaction between the cations in the present work and anions that were previously studied. The deprotonation energies show little variance, with slightly higher energies for the cations with cyclic structures. Ordering the ionic liquids investigated by decreasing average NPT energy illustrates a separation between ionic liquids that have large NPT energies and do not react hypergolically and ionic liquids that have small NPT energies and do react hypergolically. It is proposed that the trend in NPT energies and reactivity is determined by the need to balance ion concentration in the ionic liquid and the energy released by the protonation of the anion. This suggestion is supported by the recent paper by Vogl etal

In chapter 4, a description is given of the QM/MMC method that has been implemented for fully ab initio and fragment molecular orbital calculations, as well as the effective fragment potential method. In addition, the pair binding constraint has been introduced as a means of conserving chemical bonds during the MMC search by constraining only the maximum distance between pairs of bonded atoms. The secondary-Monte Carlo method was presented as a means of introducing internal molecular flexibility during the MMC search by performing a Monte Carlo search on the atoms within a unit, when the unit is moved as part of the primary MMC search. To demonstrate the QM/MMC method, the results of MMC searches were performed on the methanol pentamer using the EFP, FMO, and FAB methods, with predicted structures that are consistent with those reported previously.

The folding of n-octadecane from the elongated, all-trans conformer to the partially folded global minimum was used as a test case for pair binding an internally fragmented molecule. Although the extent of the QM/MMC simulations was not sufficient to find the folded global minimum, the method did successfully move away from a fully elongated state to a randomly distributed state and then toward the partially folded state of the global minimum without loss of chemical bonds or external biasing. The QM/MMC method provides variety of tools for investigating chemical systems for which QM accuracy is necessary but the computational cost would otherwise be too expensive.

In chapter 5, the ratio of states (ROS) method was introduced as a tool for calculating the K_{eq} of a proton transfer reaction in an aqueous or non-aqueous environment. Using pair binding to constrain a MMC search to the phase space of the

proton transfer reaction, each accepted step in the MMC search is labeled either a product state, reactant state, or neither. The weighted average of the number of product and reactant states identified over all MMC searches is used to calculate the squared ratio of the number of product and reactant states. The squared ratio is equal to the K_{eq} of the proton transfer reaction as the number of states sampled increases to the infinite step limit. To test the impact of the choice of three parameters, the proton transfer between H_2S and NH_3 with an excess attached electron has been studied using the ROS method. The choice of state sorting criterion was shown to have the largest impact on the accuracy followed by the starting configuration of the core molecules. The choice of temperature was shown to not impact the sampling of states over a range of 867 degrees Kelvin. Upon further successful testing, the ROS method can be applied to calculating the K_{eq}s of systems like ionic liquids that are otherwise prohibitively difficult to determine. The mystery of what determines whether or not an ionic liquid will react hypergolically with a strong oxidizer remains. However, a working theory of a key requirement for an ionic liquid to react hypergolically has been presented. In addition, a path has been proposed to further understanding the role that the proton transfer and ionicity play in determining hypergolicity. More importantly, the tools necessary to walk down that path have been developed and implemented in the form of QM/MMC and ROS/MMC. Building on the results of this work may well result in solving the mystery of hypergolic ionic liquids.